UC Irvine
UC Irvine Previously Published Works

Title

The response of US summer rainfall to quadrupled CO2 climate change in conventional and superparameterized versions of the NCAR community atmosphere model

Permalink

https://escholarship.org/uc/item/5zm152t9

Journal

Journal of Advances in Modeling Earth Systems, 6(3)

ISSN

1942-2466

Authors

Kooperman, Gabriel J
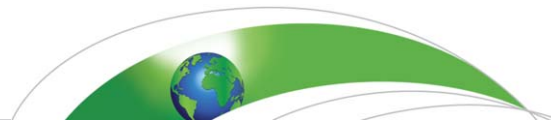Pritchard, Michael S
Somerville, Richard CJ

Publication Date

2014-09-01

DOI

10.1002/2014ms000306

Copyright Information

Peer reviewed

The response of US summer rainfall to quadrupled CO_2 climate change in conventional and superparameterized versions of the NCAR community atmosphere model

Gabriel J. Kooperman[1,2], Michael S. Pritchard[2], and Richard C. J. Somerville[1]

[1]Scripps Institution of Oceanography, University of California, San Diego, California, USA, [2]Department of Earth System Science, University of California, Irvine, California, USA

Abstract Observations and regional climate modeling (RCM) studies demonstrate that global climate models (GCMs) are unreliable for predicting changes in extreme precipitation. Yet RCM climate change simulations are subject to boundary conditions provided by GCMs and do not interact with large-scale dynamical feedbacks that may be critical to the overall regional response. Limitations of both global and regional modeling approaches contribute significant uncertainty to future rainfall projections. Progress requires a modeling framework capable of capturing the observed regional-scale variability of rainfall intensity without sacrificing planetary scales. Here the United States summer rainfall response to quadrupled CO_2 climate change is investigated using conventional (CAM) and superparameterized (SPCAM) versions of the NCAR Community Atmosphere Model. The superparameterization approach, in which cloud-resolving model arrays are embedded in GCM grid columns, improves rainfall statistics and convective variability in global simulations. A set of 5 year time-slice simulations, with prescribed sea surface temperature and sea ice boundary conditions harvested from preindustrial and abrupt four times CO_2 coupled Community Earth System Model (CESM/CAM) simulations, are compared for CAM and SPCAM. The two models produce very different changes in mean precipitation patterns, which develop from differences in large-scale circulation anomalies associated with the planetary-scale response to warming. CAM shows a small decrease in overall rainfall intensity, with an increased contribution from the weaker parameterized convection and a decrease from large-scale precipitation. SPCAM has the opposite response, a significant shift in rainfall occurrence toward higher precipitation rates including more intense propagating Central United States mesoscale convective systems in a four times CO_2 climate.

1. Introduction

The consequences of anthropogenic climate change can manifest themselves as subtle shifts in the timing or pattern of weather events leading to changes in the frequency and intensity of rainfall, which may increase drought conditions in some regions and flooding in others [*Trenberth*, 2011]. Future climate projections, including global-scale changes in precipitation patterns, from modern global climate models (GCMs) are cause for concern. There is a consensus projection of expansions of arid zones over most continents and amplification of the present-day spatial pattern of evaporation minus precipitation [*Held and Soden*, 2006; *Solomon et al.*, 2007; *Scheff and Frierson*, 2012; *Stocker et al.*, 2013]. This consensus is meaningful despite parameterization imperfections because at the very largest scales of the climate system GCMs are strongly constrained by the global energy balance and radiative properties of water vapor that are well represented across models. As a result, GCM simulations largely agree with predictions of thermodynamic theory that global precipitation should increase at a rate of 1–3% $^\circ C^{-1}$ with global warming and near-surface water vapor should increase at $\sim$7% $^\circ C^{-1}$ [*Allen and Ingram*, 2002; *Pendergrass and Hartmann*, 2014a; *Scheff and Frierson*, 2012; *Stephens and Ellis*, 2008]. At regional scales, however, future hydrologic trends in GCM projections exhibit very low confidence. Beyond the consensus on global sensitivities, GCMs using conventional statistical parameterizations of deep convection display an inability to capture the basic modes of observed variability of regional rainfall across a range of time scales [*Dai*, 2006; *Lin et al.*, 2006; *Li and Xie*, 2013], and they produce inconsistent effects of climate change on rainfall intensity [*O'Gorman and Schneider*, 2009a].

In many ways, changes in regional-scale variability and intensity of precipitation are most critical to climate change mitigation and adaptation, affecting both the availability of fresh water and the nature of extreme

conditions. A region of particular concern is the Central-Eastern United States, where GCMs disagree on even the sign of future rainfall trends [*Maloney et al.*, 2013; *Solomon et al.*, 2007; *Stocker et al.*, 2013]. Over this region, small-local and large-propagating convective systems generate the majority of summer rainfall. Propagating organized storms, known as mesoscale convective systems (MCSs), can deliver up to half of the seasonal rainfall in this important agricultural area [*Carbone and Tuttle*, 2008]. It is difficult to represent these storms in GCMs because the relevant physics includes small-scale (e.g., cold pool density currents) and large-scale (e.g., low-level jet moisture convergence) processes that straddle the divide between parameterized and explicitly resolved phenomena [*Moncrieff*, 1992]. Conventional GCMs that do not capture these mechanisms realistically (or at all) cannot assess how they may respond to climate change [*Lee et al.*, 2007]. As droughts, heat waves, forest fires, and flooding in the Central United States become more prevalent, causing significant financial impacts and loss of lives, improved projections of future changes will become increasingly critical. For example, losses in 2012 alone from droughts and heatwaves were ~$30 billion and 123 deaths, from wildfires were ~$1 billion and 8 deaths, from severe weather events were ~$11 billion and 30 deaths, and from tornadoes were ~$5 billion and 48 deaths [*Smith and Katz*, 2013] (NOAA NCDC, http://www.ncdc.noaa.gov/billions/events).

In recent years, progress has been made from both theoretical and modeling perspectives to understand changes in mean rainfall and rainfall intensity on global scales. Consistently, GCMs project that the increasing global mean precipitation trend of 1–3% $°C^{-1}$ occurs in association with a "wet-get-wetter-dry-get-drier" pattern of change, owing largely to a significant increase in specific humidity (~7% $°C^{-1}$ following the Clausius-Clapeyron relation), but only small changes in wind patterns [*Held and Soden*, 2006; *Trenberth*, 2011]. Globally, relative humidity is projected to remain fairly constant, but may vary regionally, especially over land where temperatures increase more and evaporation efficiency is limited by soil moisture, causing arid regions to become drier [*Stocker et al.*, 2013; *Trenberth et al.*, 2003]. While global mean rainfall is thermodynamically constrained, rainfall intensity in wet regions depends more on available moisture and fluctuations in low-level moisture convergence rather than on local evaporation, and is expected to scale with the increase in specific humidity at ~7% $°C^{-1}$ [*Allen and Ingram*, 2002; *Held and Soden*, 2006; *Trenberth et al.*, 2003]. This discrepancy between global mean rainfall and rainfall intensity implies that increases in heavy rain are balanced by a reduction in weak rain [*Trenberth et al.*, 2003] and less frequent storms [*O'Gorman and Schneider*, 2009a].

Observations and cloud-resolving model simulations tend to agree with the theoretical range centered on ~7% $°C^{-1}$ following the moisture increase [*Muller et al.*, 2011; *Romps*, 2011; *Stocker et al.*, 2013], but conventional GCMs simulate a smaller rate of increase in extreme rain with global warming [*Allan and Soden*, 2008; *O'Gorman and Schneider*, 2009a]. One reason for this shortcoming is the simplified representation of deep convection that does not capture organized convection and systematically rains too weakly and too often, overrepresenting the contribution of local evaporative recycling to column moisture and under-simulating the extreme tails of observed rain rates [*DeMott et al.*, 2007; *Stephens et al.*, 2010; *Sun et al.*, 2006]. Differences in precipitation rates from changes in the convective scheme can be larger than the impact of increased temperature [*Wilcox and Donner*, 2007]. However, it is common practice to apply GCMs to the problem of extreme rainfall and they have been used to develop a physical understanding of why heavy rain may not increase with moisture for all regions and seasons, due to changes in circulation, the moist adiabatic lapse rate, and temperature variability associated with when extreme rain events occur [*O'Gorman and Schneider*, 2009a, 2009b].

Some progress in estimating changes in tropical rainfall extremes has been made by relating its response to climate change to its response to interannual variability in GCMs, and constraining the relationship with satellite observations, but the estimated scaling still has a large range from 6 to 14% $°C^{-1}$ [*O'Gorman*, 2012; *Stocker et al.*, 2013]. *O'Gorman and Schneider* [2009a] argue that deficiencies in parameterized convection are mostly an issue for tropical rainfall and GCMs have a more consistent extratropical response, exhibiting a weaker increase in heavy rain than moisture (~4–6% $°C^{-1}$ from *Stocker et al.* [2013]) outside the tropics. Changes in precipitation extremes are related to upward mass fluxes that are not well represented by parameterizations of convection in the tropics where the critical updrafts are too small scale to resolve, but are better represented in the extratropics where controlled by larger-scale quasi-resolved processes such as baroclinic instability. Indeed, there is a general improvement in the realism of extreme precipitation when GCMs are run at higher resolution and the ratio of resolved to parameterized precipitation increases [*Wehner et al.*, 2010; *Kopparla et al.*, 2013]. However, in the Central-Eastern United States summer, even at higher

GCM resolution, most precipitation is generated by subgrid-scale convection. While GCMs show some agreement on annual time scales, United States summer projections remain highly uncertain [*Solomon et al.*, 2007; *Stocker et al.*, 2013]. Increases in convective available potential energy (CAPE) are expected to dominate reductions in vertical wind shear in the region under future climate change, producing overall conditions that could be more favorable to convective storms [*Stocker et al.*, 2013; *Trapp et al.*, 2009; *Brooks*, 2013]. Enhancement of the nocturnal low-level jet is also expected to increase moisture transport to the Central United States and intensify convective storms [*Patricola and Cook*, 2013b]. But the sensitivities of organized convection are likely more complicated than this, and more research is needed to explicitly link and attribute the consequences of these environmental changes to storm initiation and precipitation intensity [*Stocker et al.*, 2013].

During the North American summer, the majority of Coupled Model Intercomparison Project Phase 5 (CMIP5) GCMs project an increase in precipitation across Alaska and Northern Canada (north of ∼55°N) and along the United States east coast, and a decrease in the Northwest and Central United States, and south of 30°N over Mexico, the Gulf of Mexico, and the Western Atlantic Ocean [*Maloney et al.*, 2013; *Stocker et al.*, 2013]. Although there is some model agreement, internal variability over the Central United States summer is large, lowering confidence in the projections [*Deser et al.*, 2013]. Regional climate models (RCMs) from the North American Regional Climate Change Assessment Program (NARCCAP) similarly project increases in rainfall at high latitudes and decreases in the Northwest and Central United States, with larger regional changes than GCMs produce [*Mearns et al.*, 2013]. However, in general, there is limited statistically significant agreement in the summer in the Central United States, where different RCMs can exhibit an opposite mean precipitation change when forced by the same GCM boundary conditions, and can even produce an opposite mean response to the GCM that provided the boundary conditions. For instance, *Bukovsky and Karoly* [2011] find the NARCCAP approach, dynamically downscaling by forcing an RCM with GCM output, projects an overall decrease in rainfall in the Central United States, but captures the shift in intensity toward more extreme precipitation when the Weather Research and Forecasting (WRF) RCM is driven by the Community Climate System Model (CCSM) GCM. This result is supported by *Patricola and Cook* [2013a, 2013b] who found that enhancement of the low-level jet and nocturnal rainfall increases precipitation intensity in the Southern Great Plains in June, and a reduction in daytime rainfall in the Northern Great Plains later in the summer, lead to overall drier summer conditions. However, they note many inconclusive results including monthly differences and inconsistencies between RCMs and GCMs; overall drying in July and August is the only conclusive trend that is consistent across all models.

Increasing confidence in these projections is difficult to achieve because the impacts of higher greenhouse gas concentrations, and the subsequent response of the climate system, involve processes linked across an extremely wide range of spatial-temporal scales. GCMs that have an oversimplified representation of small-scale convective processes, whose macro-scale organization is incompletely understood, are unable to capture the observed variability and intensity of United States summer rainfall [*Lee et al.*, 2007; *Li et al.*, 2012; *Rosa and Collins*, 2013]. Yet RCM simulations that capture processes relevant rainfall extremes are subject to the boundary conditions provided to them by GCMs and do not interactively influence global-scale feedbacks, planetary circulation, and atmospheric moisture transport, all of which contribute to the regional response [*Maloney et al.*, 2013; *Wehner*, 2013]. Improving projections thus requires a realistic representation of rainfall variability across a range of spatial-temporal scales, and a modeling framework that maintains links to global feedbacks and changes in large-scale circulation.

A new type of climate model is gaining traction, which addresses both of these issues by explicitly resolving small-scale cloud physics with cloud-resolving models (CRMs) embedded in a GCM, improving the representation of multiscale cloud processes and rainfall variability compared to observations in the present climate. This approach, called superparameterization (SP), was first implemented in the National Center for Atmospheric Research (NCAR) Community Atmosphere Model (CAM) version 3.0 [*Khairoutdinov and Randall* 2001, 2003; *Khairoutdinov et al.*, 2008] and through collaboration between the Center for Multiscale Modeling of Atmospheric Processes (CMMAP) and the Pacific Northwest National Laboratory (PNNL), has recently been implemented in CAM version 5.0 (CAM5) [*Randall et al.*, 2003; *Wang et al.*, 2011]. Early work has shown significant improvement in the representation of rainfall statistics with superparameterization when model results are compared with measurements taken at the United States Department of Energy, Atmospheric Radiation Measurement, Southern Great Plains (SGP) site. Probability density functions (PDFs) of summer

rain rates at SGP show that SPCAM captures the observed contribution from heavier rain rates to accumulated seasonal precipitation (i.e., these PDFs in CAM drop off at $\sim$20 mm d^{-1}, but extend past $\sim$40 mm d^{-1} in both the observations and SPCAM). This improves rain penetration through the land-surface vegetation canopy, reducing local re-evaporation recycling, which occurs in CAM due to weak rain rates and thus exaggerates mean seasonal rainfall [*DeMott et al.*, 2007]. In addition to improvements in intensity, the diurnal timing of rainfall in SPCAM is also in better agreement with observations both at the SGP site and over all boreal summer land, shifting the peak timing to later evening hours and reducing the diurnal amplitude relative to CAM, whose convection is too tightly bound to the solar cycle [*DeMott et al.*, 2007; *Pritchard and Somerville*, 2009]. A broader analysis of rainfall variability over the United States shows that SPCAM improves the representation of both light and heavy rain, especially in regions where the fraction of rainfall from parameterized convection is greatest [*Li et al.*, 2012]. In general, CMIP5 GCMs trigger convection too frequently, oversimulating moderate rain, and under-simulating weak and heavy rain compared to observations and SPCAM [*Rosa and Collins*, 2013].

The superparameterization approach also gives rise to self-organized convective systems in the tropics and midlatitudes, whose emergent large-scale behavior has been difficult to represent in parameterized GCMs with simplified physics. A strong mesoscale convective system (MCS) signal has been found in several versions of SPCAM [*Pritchard et al.*, 2011; *Kooperman et al.*, 2013]. *Kooperman et al.* [2013] show this signal is most realistic in the newest SPCAM version based on CAM5, using a new physically based index to composite MCS statistics in the Central United States. The index isolates strong eastward propagating convection, and with a simple set of criteria, identifies MCS events and composites their propagation by phase. In an early version of SPCAM (3.5), MCS anomalies were unrealistically large scale and concentrated, while surface rainfall was too weak. SPCAM version 5, with high-order microphysics, improves the signal, producing a composite storm in which the spatial extent, the magnitude of longwave cloud forcing, and the colocated timing of rainfall are all in better agreement with observations. It is still an open question as to which aspects of an explicit representation of the meso-beta scale are critical to improved performance of superparameterized models over the Central United States and missing from conventional GCMs. But there are several compelling features of the SPCAM design. *Pritchard et al.* [2011] discuss new pathways introduced by the embedded CRM such as the ability to evolve a second baroclinic convective heating response to a vertically sheared large-scale environment [*Moncrieff*, 2010], including local effects of cold pools and evaporative downdrafts [*Carbone et al.*, 2002]. Memory of subgrid-scale organization persisting across GCM time steps may play an important role in enabling SPCAM's MCS signal [*Mapes and Neale*, 2011], as well as enhanced sensitivity to free tropospheric moisture variations [*Thayer-Calder and Randall*, 2009], but this has not been explicitly tested.

To date, the superparameterized model MCS signal and United States summer rainfall have only been evaluated in present-day climate. The computational expense of explicitly resolved convection adds an additional challenge for century-long climate change integrations. In the present study, a time-slice experiment design is implemented, employing atmosphere-only SPCAM climate change simulations driven by sea surface temperature and sea ice boundary conditions from the fully coupled Community Earth Systems Model (CESM, with CAM as the atmospheric component), to address several unanswered questions: How will precipitation in the Central-Eastern United States respond to higher greenhouse gas concentrations? Will the climate change perturbation project onto natural patterns of rainfall or will it shift the system to a new precipitation regime? Will organized convective storms become more or less intense in a warmer world? How does the representation of convection influence changes in rainfall intensity as well as the mean precipitation response?

The remainder of this paper is separated into four main sections. Section 2 gives a brief description of the models used in the experiment, their configurations, and the simulation design. The results and discussion are divided into section 3 presenting the mean rainfall response and associated large-scale circulation, and section 4 evaluating changes in rainfall and convective storm intensity. The main conclusions and future work are summarized and discussed in section 5.

2. Models and Experiment Setup

2.1. Community Atmosphere Model
Conventional and superparameterized versions of the NCAR Community Atmosphere Model (CAM) are evaluated for this experiment. CAM is the atmospheric component of the fully coupled Community Earth

System Model (CESM), which also includes interactive ocean, sea ice, and land-surface models. When run as a stand-alone atmospheric GCM, CAM is forced by prescribed monthly mean sea surface temperature and sea ice boundary conditions from either observations or coupled CESM output, with an interactive land surface. CAM version 5 is used in this study, which includes an updated *Zhang and McFarlane* [1995] parameterization of deep convection based on a dilute plume CAPE closure with convective momentum transport, the University of Washington shallow convection scheme with moist turbulence [*Park and Bretherton*, 2009], two-moment cloud microphysics [*Morrison and Gettelman*, 2008], and interactive aerosol-cloud and aerosol-radiation processes [*Liu et al.*, 2012]. In this study, CAM was run with a finite volume dynamical core, at a standard 1.9° (latitude) by 2.5° (longitude) horizontal resolution with 30 vertical levels. Climatological monthly mean boundary conditions were generated from CESM output and are described in the experiment setup section below. For more details, see the official CAM scientific description by *Neale et al.* [2010].

2.2. Superparameterization

In SPCAM, the conventional statistical parameterizations for clouds and boundary layer processes are replaced with simplified (two-dimensional and periodic boundary conditions) cloud-resolving models (CRMs) [*Randall et al.*, 2003]. An independent CRM is embedded in each column of CAM to explicitly resolve cloud processes. The CRM is linked to large-scale GCM-resolved dynamics following a similar implementation as conventional parameterizations, i.e., CAM supplies the CRM with large-scale heating, moistening, and circulation tendencies, and the CRM returns a subgrid convective response [*Grabowski*, 2001; *Benedict and Randall*, 2009]. This aspect of SPCAM explicitly accounts for subgrid variability and introduces memory in aerosol, cloud, radiation, and precipitation processes [*Khairoutdinov et al.*, 2005; *Pritchard et al.*, 2011; *Wang et al.*, 2011]. Independent CRMs with periodic boundary conditions make SPCAM vastly more scalable on current supercomputers, but add 200 times more computational expense relative to CAM [*Khairoutdinov et al.*, 2005]. In SPCAM version 5 used here, GCM-scale aerosol fields are evolved by CRM-scale statistics of cloud processes including vertical updraft velocity, humidity, and precipitation; and each CRM column produces an independent realization of cloud droplet activation and aerosol humidification [*Wang et al.*, 2011]. The GCM configuration for SPCAM is the same as described for CAM above (1.9° by 2.5° with 30 vertical levels), and the CRM is aligned in north-south orientation with 32 columns at 4 km horizontal resolution and 28 vertical levels colocated with the bottom 28 levels in CAM. For additional details see *Wang et al.* [2011].

2.3. Experiment Setup

The added computational expense of resolved convection, two-moment cloud microphysics, and interactive aerosol in SPCAM version 5 makes fully coupled (interactive ocean and sea ice) century-long climate simulations impractical on current supercomputing hardware. However, the shared large-scale atmospheric (dynamics), land, ocean, and sea ice components with CESM/CAM, provide a framework where much can be learned from short (multiyear) atmosphere-only time-slice experiments driven by initial (atmosphere and land) and boundary (sea surface temperature and sea ice) conditions from CESM/CAM simulations. For this study, initial and boundary conditions for CAM and SPCAM were created from a pair of preindustrial (PI) and abrupt four times (4×) CO_2 simulations run as part of CMIP5. Climatological monthly mean sea surface temperature and sea ice boundary conditions are based on the last 25 years of each CESM simulation, years 26–50 for PI and 126–150 for 4×, as shown by blue and red lines in Figure 1a, respectively.

By the end of the abrupt 4×CO_2 simulation, global-annual mean surface temperature has increased by more than 5°C as seen in Figure 1a and global-annual mean precipitation has increased by 7.6%. The coupled climate system is nearly 80% adjusted to the 4×CO_2 forcing and will ultimately reach an equilibrium increase of ~7°C, estimated following a linear regression approach [*Andrews et al.*, 2012; *Gregory et al.*, 2004]. Regional annual sea surface warming anomalies (4× − PI) are as large as 8.4°C and there is an annual reduction of up to 50% of sea ice over the entire Arctic (less only near the edges where annual sea ice is already less than 50%) shown in Figures 1b and 1c. Regional sea surface temperature anomalies are even larger on a seasonal timeframe, reaching as high as 12.0°C for boreal summer (May, June, July, August— MJJA), with a 60% loss of total Arctic seasonal sea ice coverage. The only region that shows a reduction in sea surface temperature is off the southeast coast of Greenland, due to increased fresh melt water input and a slowdown of deepwater formation and Atlantic meridional overturning circulation [*Stocker et al.*, 2013; *Stouffer et al.*, 2006]. Warming is considerably higher over land than ocean and is amplified at higher
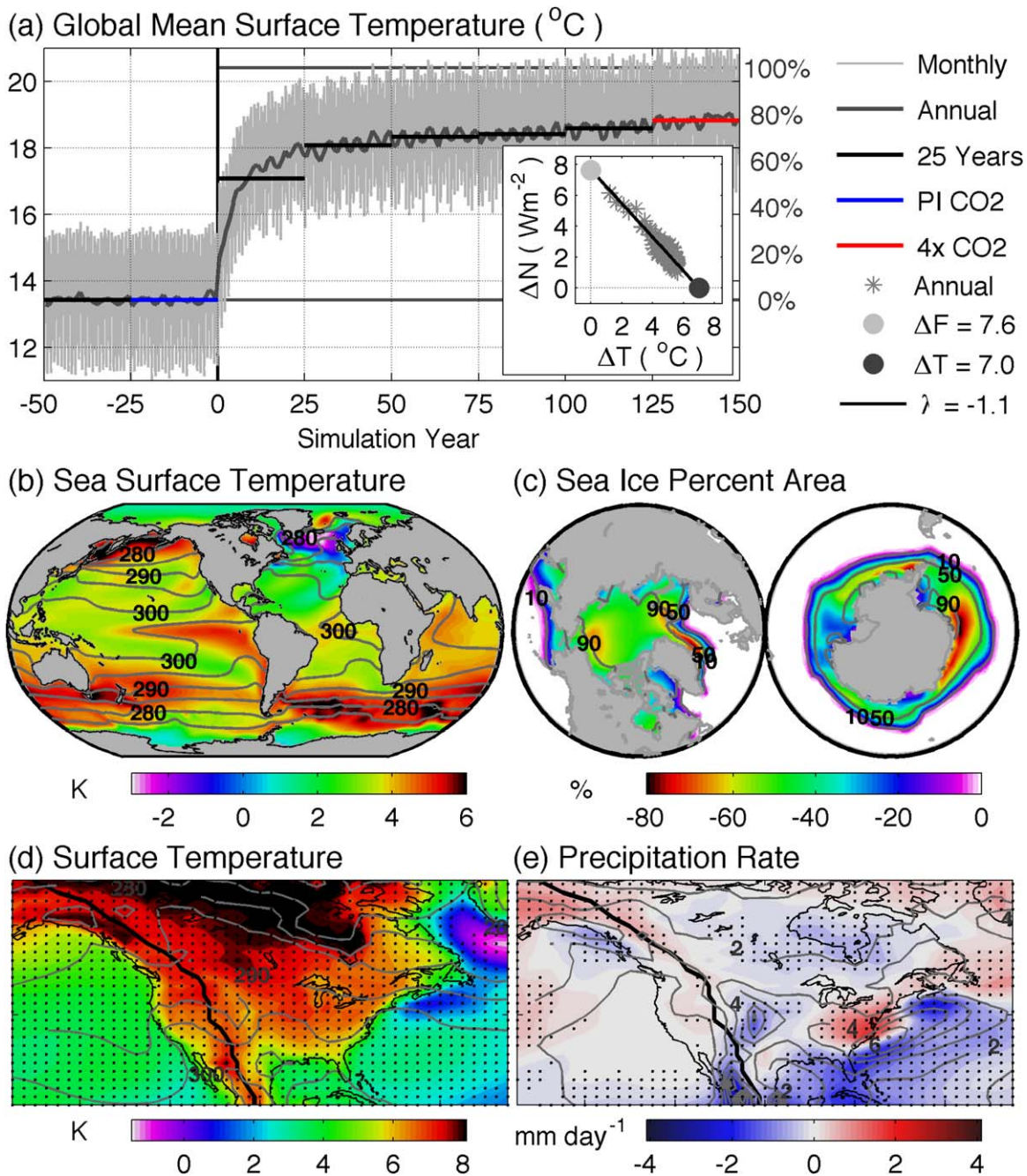
Figure 1. CESM results for (a) global mean surface temperature and the linear regression of global-annual mean surface temperature on the top-of-atmosphere flux imbalance (small plot); 25 year PI mean (contours) and the difference between 4× and PI (colors) for (b) sea surface temperature (PI intervals of 5 K), (c) sea ice percent area (PI intervals of 40%), (d) seasonal (MJJA) mean surface temperature (PI intervals of 5 K), and (e) seasonal (MJJA) mean precipitation rate (PI intervals of 1 mm d^{-1}); blue and red lines in Figure 1a show 25 year averaging periods used in Figures 1b–1e; vertical black line in Figure 1a shows abrupt transition to 4×CO$_2$; and solid black line shows Rocky Mountain ridgeline and stippling indicates statistical significance at 90% confidence in Figures 1d and 1e.

latitudes [*Solomon et al.*, 2007; *Stocker et al.*, 2013], as seen for the boreal summer over North America in Figure 1d.

Seasonal mean precipitation changes over North America projected by the coupled CESM simulations show significant regional variability. Rainfall is enhanced over Alaska and Northwest Canada and the Eastern United States consistent with CMIP5 ensemble projections [*Maloney et al.*, 2013; *Stocker et al.*, 2013]. There is a weak increase in rainfall west of the Rockies and a decrease in the Central United States, across Northeast Canada, and the Gulf of Mexico, regions where CMIP5 models do not have statistically significant

agreement of future precipitation changes [*Stocker et al.*, 2013]. Although not statistically significant, the ensemble mean changes and the majority of models also indicate a reduction in precipitation in the Central United States consistent with CESM, but show a decrease in the west opposite to that of CESM [*Maloney et al.*, 2013; *Stocker et al.*, 2013].

The question naturally arises as to what extent these rainfall projections may have been an artifact of conventional convection parameterization, and whether they are robust to an explicit representation of convection. To address this, our experiment setup follows a straightforward time-slice design. A set of four 5 year boreal summer (MJJA) simulations with CAM and SPCAM were run with PI (284.7 ppm) and 4× (1138.8 ppm) CO_2 concentrations and climatological sea surface temperature and sea ice boundary conditions, as described above. To minimize computational expense and divergence in the land component of the models (sea surface temperature and sea ice are constrained by prescribed conditions), only the summer season was run for SPCAM, which was initialized from the same spring conditions as CAM. This was achieved by running a set of 6 year simulations with CAM initialized from land and atmosphere conditions taken from the end of CESM PI and 4×CO_2 runs. Neglecting the first year, SPCAM and CAM (for consistency) were reinitialized from these base simulations each April for the subsequent 5 years and integrated through August; three-hourly average output for May through August were analyzed for this experiment.

Constraining the long-term climate state of CAM and SPCAM in this fashion helps to isolate the role of explicitly resolved convection, but it also introduces some limitations worth mentioning. For instance, the treatment of convection may influence the strength of climate feedbacks (e.g., changes in longwave emission associated with the increase in water vapor transported to high altitudes) that ultimately determine the global-scale response of the system. Our approach inherently masks potential differences in the response that could impact global mean surface warming or planetary-scale circulation patterns on these longer time scales. However, these differences can make it difficult to disentangle cause and effect on seasonal and regional scales. The approach used here is aimed at isolating the impact of resolved versus parameterized convection on United States boreal summer climate. Much like the RCM climate change simulation paradigm, in this experiment design SPCAM is subject to the initial and boundary conditions provided by an independent model—CAM. But unlike RCM climate projections, global-scale circulation and feedbacks are not constrained by lateral boundary conditions, and planetary energetics can play an important role in producing the overall regional response, notwithstanding controlled SSTs.

3. Influence of Large-Scale Dynamics on Mean US Rainfall Response

3.1. Changes in Mean Summer Rainfall

Reassuringly, the main features of the mean United States rainfall response in the fully coupled CESM reference run, discussed above, are replicated in our CAM boundary-driven time-slice simulation shown in Figure 2a. These include an increase in rainfall over Alaska and Northwest Canada and the Eastern United States, and a decrease in the Central United States, Northeast Canada, south of Florida, east of the Gulf Stream, and off the Northeast United States coast. These anomalies are statistically significant at 90% confidence with respect to both 25 year monthly mean variability in CESM (Figure 1) and 5 year three-hourly variability in CAM (Figure 2).

Superparameterization produces an interesting effect on the summer rainfall climate change signal over the United States. Figure 2b shows that SPCAM captures a similar, but weaker, rainfall increase over Alaska and the Northwest United States, decrease over Northeast Canada, and little overall change in the Southwest. However, opposite to CAM, SPCAM predicts a *rainfall decrease* over the entire Eastern United States, which is most pronounced over the Gulf Stream and southern Gulf states. And unlike CAM, SPCAM projects a small *increase* in rainfall extending from Texas into the Central United States through Missouri. Even though this is a noisy region for detecting shifts in convective variability (due to interannual and seasonal variations in the preferred zone of summer storm propagation) a statistically significant change is evident in the 5 year simulation sample. Understanding intermodel differences in these climate change anomalies requires understanding the effect of superparameterization on both the baseline (PI) and 4×CO_2 end members. The large reduction in precipitation over the Gulf Stream in SPCAM coincides with a strong regional maximum there in the PI simulations, which is reduced by nearly half in the 4×CO_2 simulation. The Central United States rainfall reduction in CAM also coincides with a local modulation of a regional PI maximum in
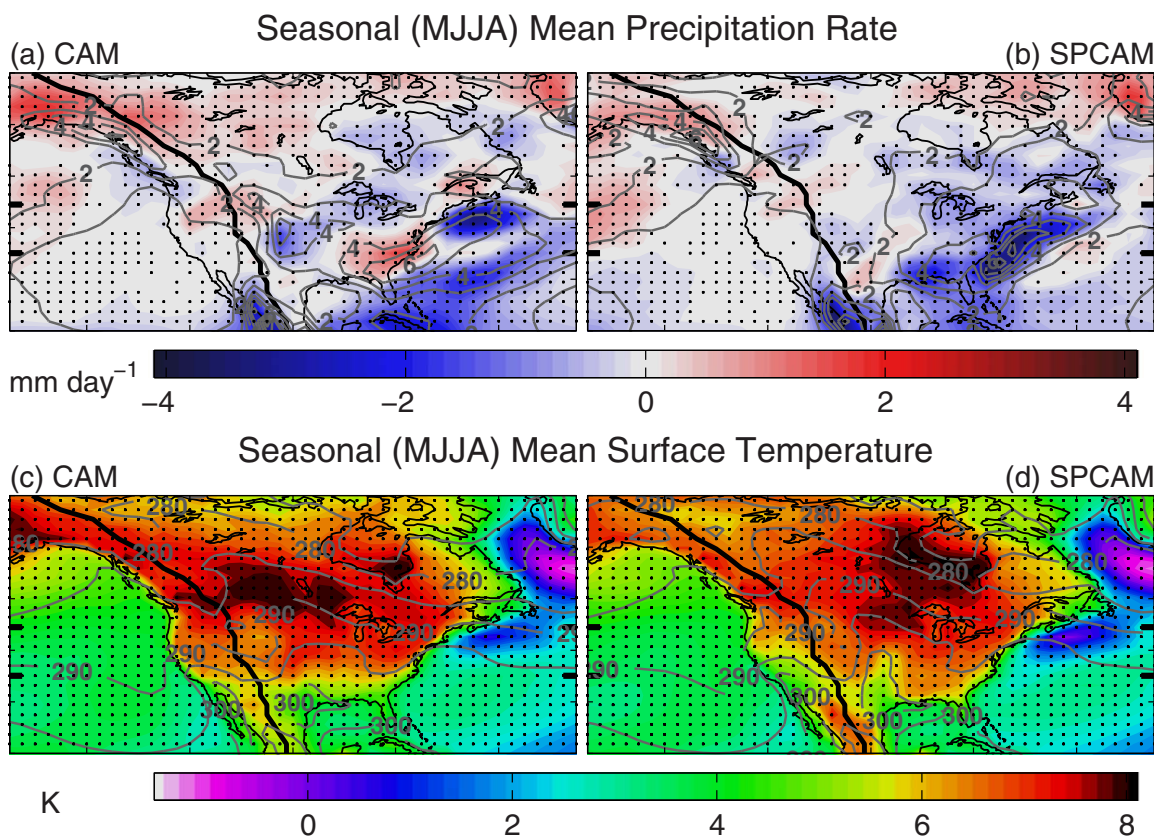
Figure 2. A 5 year seasonal (MJJA) mean PI (contours) and the difference between 4× and PI (colors) (a and b) precipitation rate (PI intervals of 1 mm d^{-1}) and (c and d) surface temperature (PI intervals of 5 K) from (Figures 2a and 2c) CAM and (Figures 2b and 2d) SPCAM simulations; black line shows Rocky Mountain ridgeline; stippling indicates statistical significance at 90% confidence.

that model, whereas the east coast response appears to be linked to an onshore shift in a local maximum of offshore rainfall.

These differences in the mean precipitation response between the two models develop despite the fact that they produce similar large-scale surface (2 m) temperature changes shown in Figures 2c and 2d. As expected, temperature over the sea surface is well constrained by the prescribed boundary conditions and is nearly identical in both models. Both models also show greater warming over land and at higher latitudes consistent with CMIP5 projections [*Stocker et al.*, 2013]. There are regional differences in the patterns of warming over land, especial over Canada, but the magnitudes are comparable, reaching as high as 8°C in northern Canada. The temperature change in the time-slice simulations is slightly lower over land than in CESM, which has greater warming at high latitudes and extending south along the Rocky Mountain ridgeline, but the general patterns are represented in both models.

Changes in column water also highlight differences in the seasonal mean responses of CAM and SPCAM. Both project an overall increase in precipitable water, but with minimum increases over Northern Mexico and along the Rocky Mountain ridgeline, off the northeast coast of Canada, and in the Western Atlantic Ocean south of 25°N seen in Figures 3a and 3b). Some key regional nodes of rainfall modulation are coupled to supportive local vapor tendencies. For instance, water vapor in CAM is enhanced in the region of maximum increase in precipitation along the Eastern United States coast. A weaker local increase in water vapor in SPCAM occurs in the Central United States, coincident with a small increase in precipitation there. Both models have a significant reduction in liquid water path in the Central-Eastern United States and little change west of the Rockies (Figures 3c and 3d). Reductions in seasonal mean liquid water path extend north of 70°N in SPCAM, but begin to increase significantly in CAM north of 60°N. Ice water path (Figures 3e and 3f) in CAM is reduced everywhere except the Central-Eastern United States and exhibits a similar increase over the Eastern United States and decrease off the northeast coast as precipitation. In
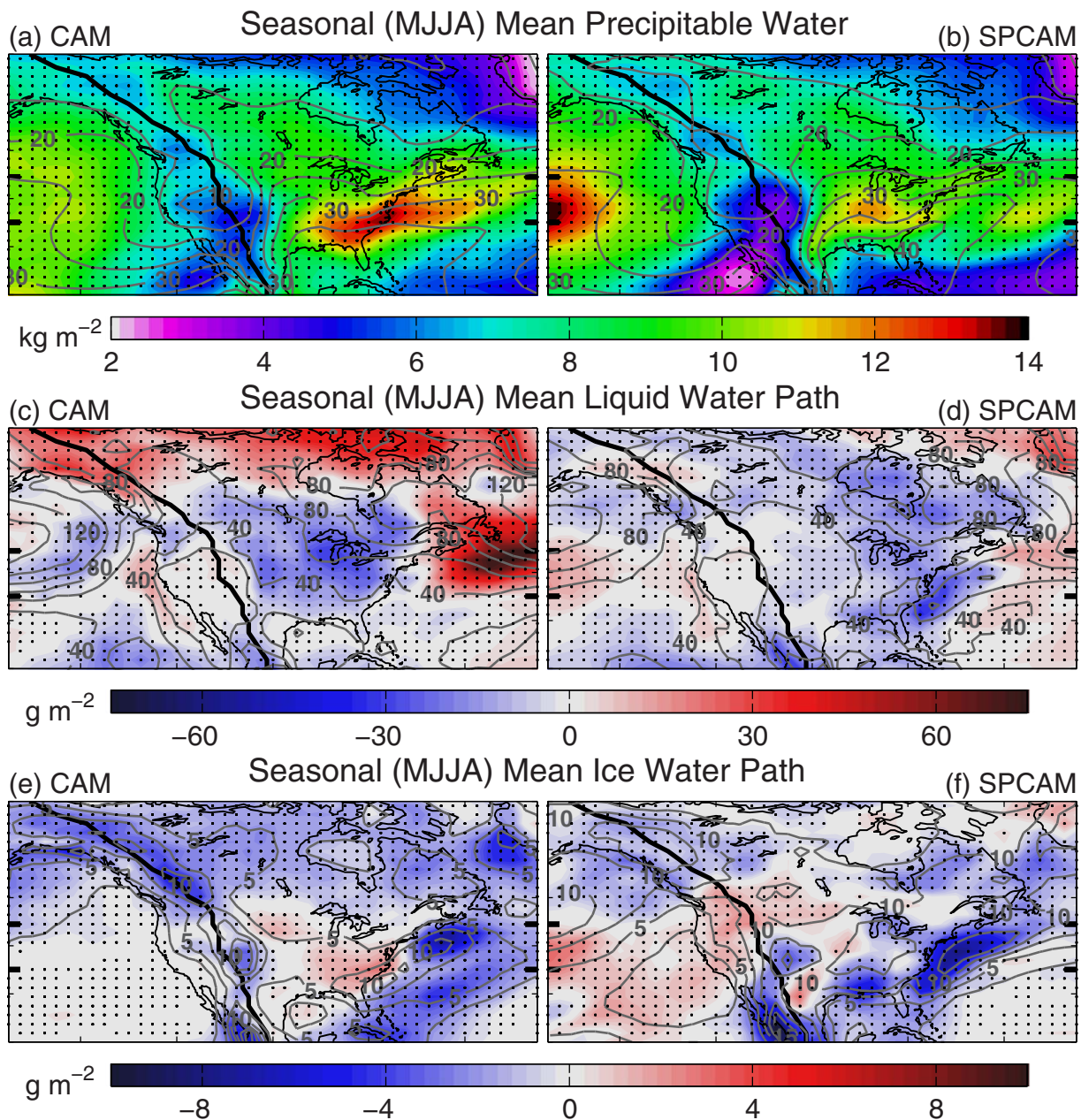
Figure 3. A 5 year seasonal (MJJA) mean PI (contours) and the difference between 4× and PI (colors) (a and b) precipitable water (PI intervals of 5 kg m^{-2}), (c and d) liquid water path (PI intervals of 20 g m^{-2}), and (e and f) ice water path (PI intervals of 2.5 g m^{-2}) from (Figures 3a, 3c, and 3e) CAM and (Figures 3b, 3d, and 3f) SPCAM simulations; black line shows Rocky Mountain ridgeline; stippling indicates statistical significance at 90% confidence.

SPCAM changes in ice water path also show similar patterns as precipitation, with a large decrease over the Gulf Stream and Gulf states, and increase from Texas up through the Central United States and Northwest United States. In both models increased rainfall over Alaska coincides with reduced ice water path and increased liquid water path.

3.2. Regional and Planetary Circulation Anomalies

It is logical to expect that some of the changes in mean precipitation and column water described above are associated with dynamical differences in the response to boundary forcing between the two models, both on planetary and regional scales. Consistent with this view, although mean surface temperature changes over the United States are similar (Figures 2c and 2d), higher in the atmosphere the thermal state
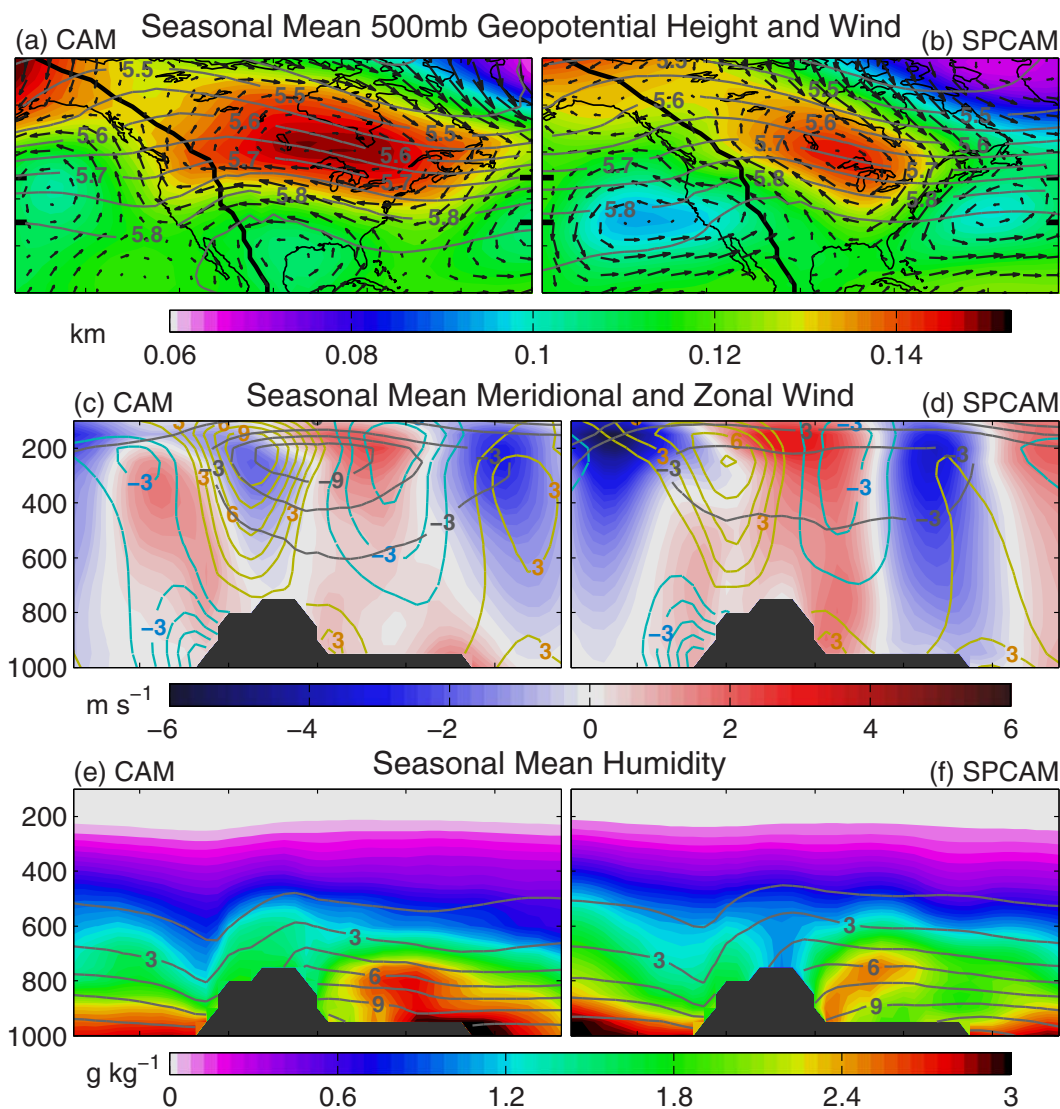
Figure 4. A 5 year seasonal (MJJA) mean PI (contours) and the difference between 4× and PI (colors) (a and b) 500 mb geopotential height (PI intervals of 0.05 km) and the change in horizontal wind (vectors); and meridional (35–45°N) mean (c and d) meridional wind (colors and PI contours—blue-negative and yellow-positive—in intervals of 1.5 m s⁻¹) and the change in zonal wind (black contours in intervals of 3 m s⁻¹), and (e and f) specific humidity (PI intervals of 1.5 g kg⁻¹) from (Figures 4a, 4c, and 4e) CAM and (Figures 4b, 4d, and 4f) SPCAM simulations; left and right y axis tick marks in Figures 4a and 4b show meridional averaging region for Figures 4c–4f, black area (line in Figures 4a and 4b) indicates Rocky Mountains.

between the models diverges, resulting in substantial differences in the placement and magnitude of regional circulation and moisture anomalies. The anomalies seen in the 500 mb geopotential height field (Z_{500}), shown in Figures 4a and 4b, are also seen in the structure of geopotential height at higher pressure levels closer to the surface (not shown). Increased atmospheric temperature and thermal expansion cause the geopotential height field to rise over the entire domain, but changes in the meridional temperature gradient (baroclinicity), topographic heating, and land-sea contrast can create regional anomalies of enhanced ridging. Both models have minima over the Northeast Pacific Ocean and east of Greenland, and maxima over Alaska and Eastern North America.

A particularly interesting effect of superparameterization is the weaker localized ridging downstream (east) of the Rockies in response to the 4×CO₂ forcing. Although both models predict strong localized ridging just east of the Rockies, this effect is much greater in CAM than SPCAM, and extends further off the continent over the Northwest Atlantic Ocean. This discrepant sensitivity may in turn be linked to different degrees of mountain-wave coupling in the models' mean state. A general effect of superparameterization

not noted previously is a muting of the baseline stationary wave jet streak in the lee of the Rockies relative to CAM, in both the PI and $4 \times CO_2$ simulation end members (not shown). CAM's exaggerated ridging response to $4 \times CO_2$ is colocated with its exaggerated mean state jet streak. In turn, associated circulation anomalies over the United States east coast promote onshore southeasterly flow (warm moist marine air) in CAM, but northerly flow (cold dry continental air) in SPCAM. In both models, there is anomalous southerly flow (low-level jet-warm moist air) from the Gulf of Mexico into the Central United States, but it is greater in SPCAM than CAM. Such flow patterns could lead to differences in moisture convergence contributing to the patterns of precipitable water anomalies in Figures 3a and 3b) and coincident mean precipitation changes in Figures 2a and 2b) as discussed above: an increase in the Eastern United States and decrease in the Central United States in CAM; and the opposite increase in the Central United States and decrease in the Eastern United States in SPCAM.

Geopotential height anomalies due to the $4 \times CO_2$ forcing tend to tilt toward the northwest with height, and changes are even greater in CAM than SPCAM higher in the atmosphere, in association with a larger temperature increase at lower pressure levels. In general, 500 mb circulation changes in the Central-Eastern United States are similar to near-surface changes, which also show southeasterly flow in CAM and northerly flow in SPCAM along the United States east coast, and stronger southerly flow into the Central United States in SPCAM; although the magnitude is larger and has a stronger easterly component in both models at 500mb. Anomalous easterly flow is part of an overall weakening of the zonal jet, depicted in the black contours in Figures 4c and 4d), which is regionally more striking, and weakens more significantly in CAM than SPCAM, reducing vertical wind shear over the Central United States. As mentioned earlier, the zonal jet is much stronger in the baseline (PI) CAM simulation and undergoes significant local modulation due to warming, whereas in SPCAM, it shifts to the east rather than weakening. The impact of superparameterization on mountain-stationary wave dynamics has not been explored in detail, but may have important consequences for baseline regional circulation and differences in the response to climate change seen here. These differences are also seen in the weakening of the stationary meridional wind field (which results from topographic anticyclonic circulation generated by the Rocky Mountains) in CAM as the $4 \times CO_2$ anomalies project onto the PI patterns, also reducing vertical wind shear. However, in SPCAM, the meridional wind anomalies appear to be less phase-locked to PI patterns than in CAM and tend to shift the position rather than weaken meridional flow with $4 \times CO_2$. Also in SPCAM, stronger meridional wind anomalies extend down to the surface east of the Rocky Mountains, in association with enhanced near-surface southerly flow (low-level jet) into the Central United States and northerly flow along the east coast (Figure 4d). This is coincident with the elevated humidity pattern that lifts up from the eastern slope of the Rockies to reach levels above 700 mb in the Central United States seen in Figure 4f. In CAM, enhancement of the Central United States low-level jet is weaker and a broader southerly flow below 600 mb extends over the east coast, associated with a larger increase in humidity further east (Figure 4e) than in SPCAM.

On larger spatial scales, another interesting effect of superparameterization is a reduction in the magnitude of polar amplified warming. The above regional circulation changes over North America are connected to a larger planetary response to the $4 \times CO_2$ forcing. For example, the regional peak in the Z_{500} anomaly over North America shown in Figures 4a and 4b) between $50°$ and $60°N$ is also seen in the zonal mean Z_{500} field (Figure 5b). Both models increase Z_{500} by more than 100 m globally due to significant atmospheric warming, but the increase in CAM is much larger north of $30°N$, reaching a maximum difference of 50 m at the north pole relative to SPCAM. The large Z_{500} anomaly north of $70°N$ in CAM results from a much greater increase in Arctic temperature throughout the atmospheric column (Figures 5c and 5d).

It is natural to wonder how superparameterization could result in such a striking difference in polar amplification, and how this might impact the Central United States region. While surface temperature over the ocean is well constrained by prescribed sea surface temperatures in both models, differences in the warming over land, sea ice, and higher in the atmosphere result in higher total (land, ocean, and ice) Arctic warming in CAM (up to $1.5°C$ greater than SPCAM). In turn, atmospheric warming causes changes in the geopotential height field, which impacts local and nonlocal (including Central United States) circulation. For instance, higher Z_{500} over the pole is associated with a southward pressure gradient force anomaly, which in combination with a strong Coriolis force, maintains increased easterly flow in the Arctic, not seen in SPCAM (Figures 6a and 6b). Similarly, on the southern side of the midlatitude geopotential height anomaly ($50–60°N$), there is a stronger increase in easterly flow (slow down of the zonal jet) in CAM throughout the atmospheric column, consistent
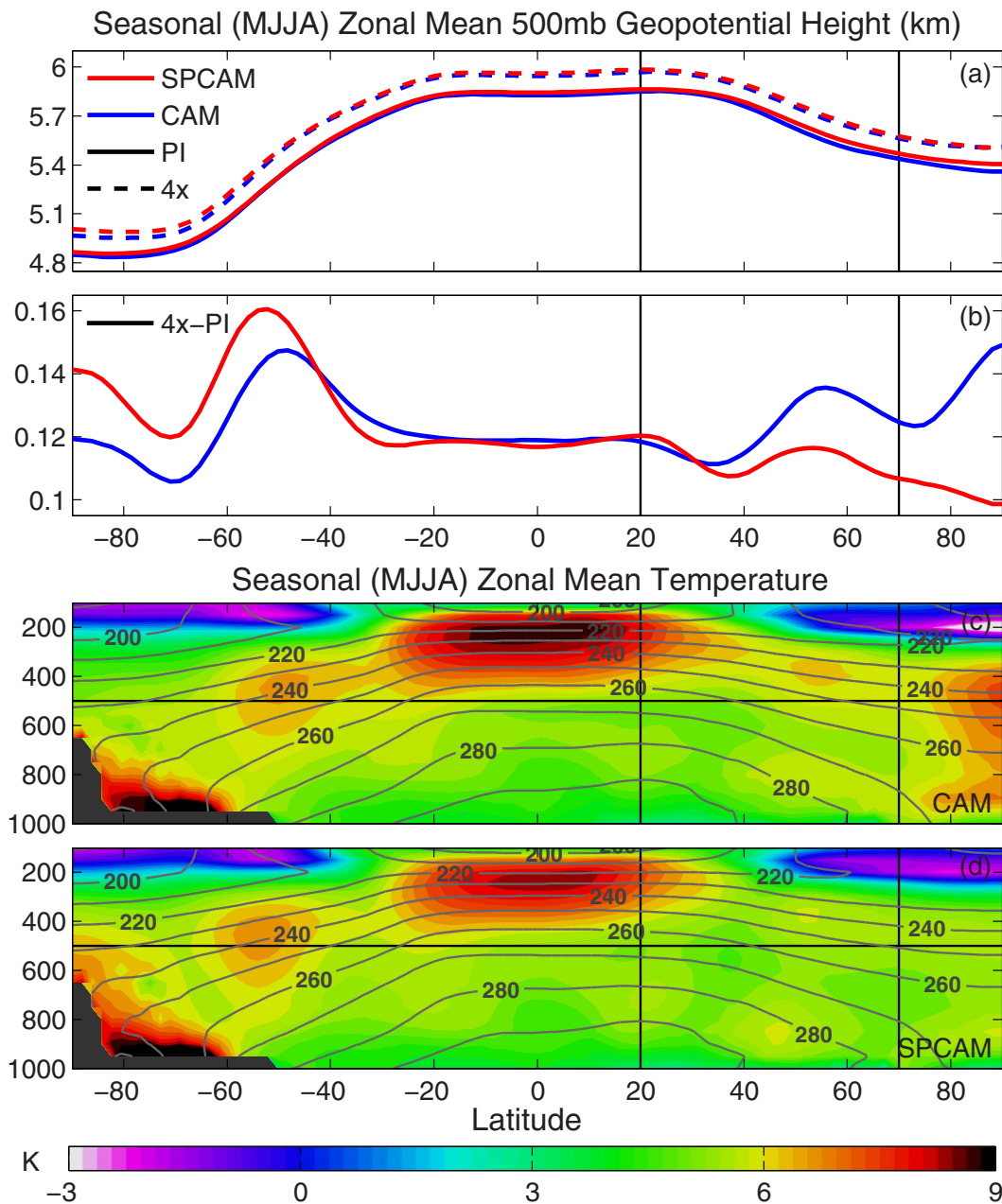
Figure 5. A 5 year seasonal (MJJA) zonal (a) mean (PI-solid, 4×-dash) and (b) the difference between 4× and PI 500 mb geopotential height, and (c and d) PI (contours) and the difference between 4× and PI (colors) temperature (PI intervals of 10 K) for (Figure 5c, blue) CAM and (Figure 5d, red) SPCAM simulations; vertical black lines show the meridional range of Figures 2 and 3; horizontal black lines in Figures 5c and 5d are 500 mb.

with reduced zonal flow across North America seen in Figures 4c and 4d). These changes in the Z_{500} field and zonal mean circulation affect the strength, shift the center (maximum), and broaden the extent of the PI zonal jet structure. In general, CAM exhibits a greater expansion and weakening of zonal mean flow, while SPCAM exhibits a greater shift in the meridional position. Both models show an upward and southward shift and broadening of the northern hemisphere zonal mean jet, seen as a reduction in westerly flow between 40° and 55°N below 200 mb, and an increase to the north and south. In CAM, the jet weakens and broadens more, with an increase in westerly wind reaching as far south as 15°N.

Anomalous counterclockwise flow in the pressure-latitude plane (negative stream function) also stretches further south in CAM, reducing northerly surface wind associated with the summer mean PI Hadley circulation and the export of extratropical moisture between 15° and 30°N, shown in Figures 6c and 6d. Although
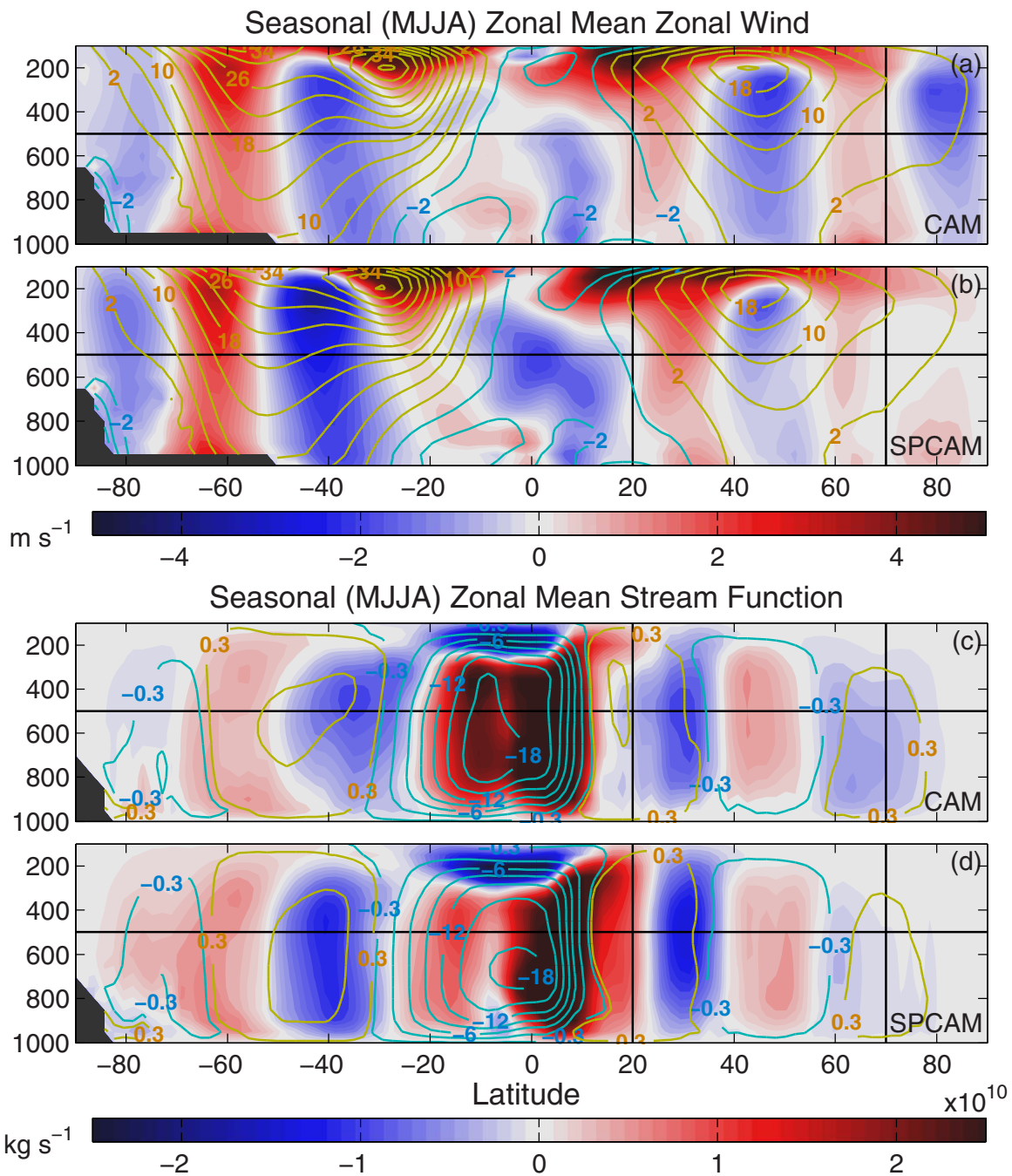
Figure 6. A 5 year seasonal (MJJA) zonal mean PI (blue-negative and yellow-positive contours) and the difference between 4× and PI (colors) (a and b) zonal wind in m s^{-1} (PI intervals of 4 m s^{-1}) and (c and d) meridional stream function in 10^{10} kg s^{-1} (PI intervals of 3 × 10^{10} kg s^{-1} after the first 0.3 × 10^{10} kg s^{-1} contour) for (Figures 6a and 6c) CAM and (Figures 6b and 6d) SPCAM simulations; vertical black lines show the meridional range of Figures 2 and 3; horizontal black lines are 500 mb.

less broad, the circulation anomalies south of 20°N (easterly zonal and clockwise-meridional flow) and from 20° to 40°N (westerly zonal and counterclockwise-meridional flow) are larger in SPCAM than CAM, indicating a stronger shift and less weakening of the circulation. Overall, these changes represent a widening and weakening of the Ferrel circulation and reduction in the northward extent of the Northern Hemisphere summer Hadley circulation. Hadley circulation also weakens, rises, and expands further south in the Southern Hemisphere. These planetary-scale changes including weakening of the jet, reduction of the meridional temperature gradient (polar amplification), and a shift in the position of the midlatitude baroclinicity
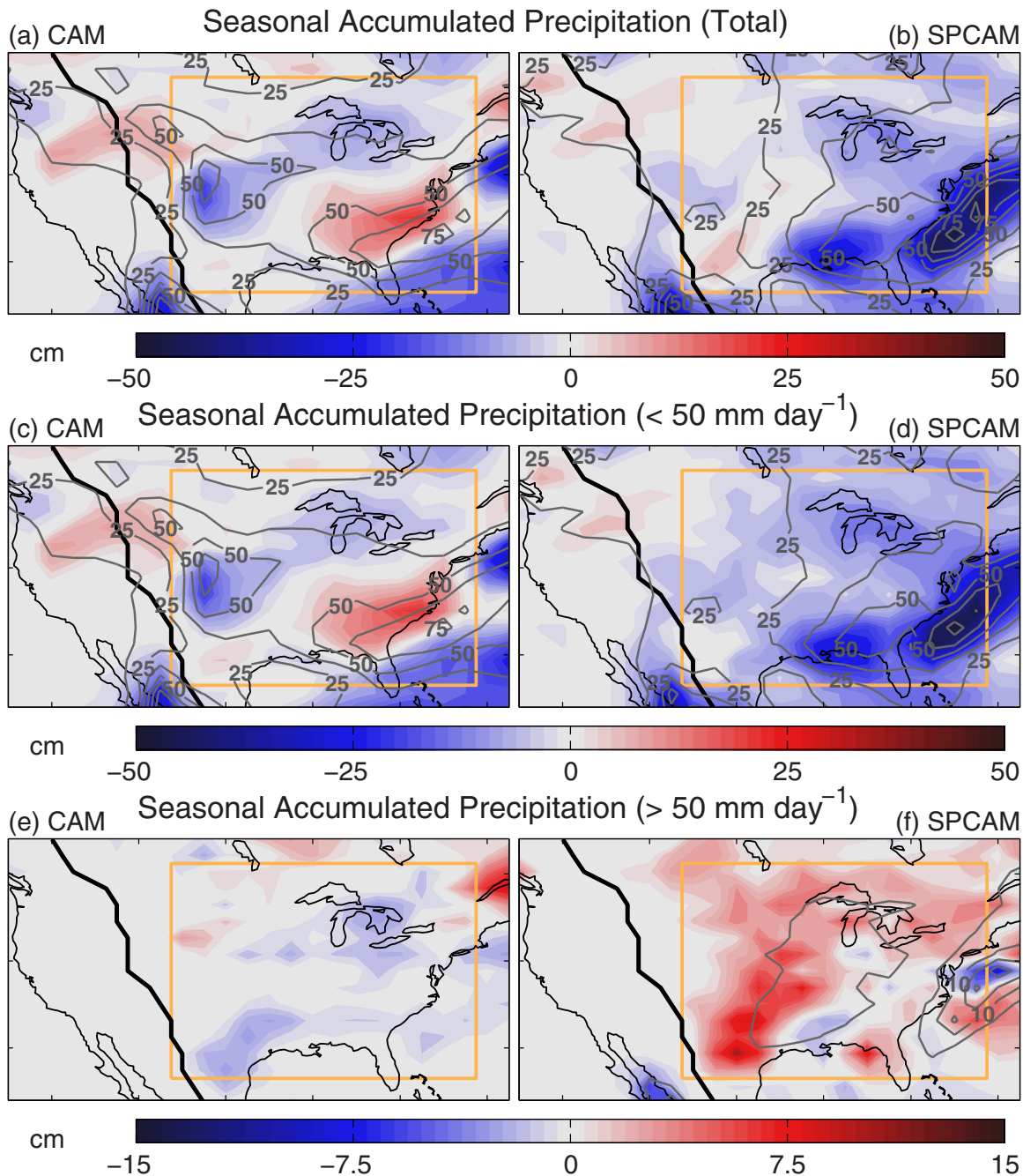
Figure 7. A 5 year seasonal (MJJA) PI (contours) and the difference between 4× and PI (colors) (a and b) total accumulated precipitation (PI intervals of 12.5 cm), (c and d) accumulated precipitation from rates less than 50 mm d^{-1} (PI intervals of 12.5 cm), and (e and f) accumulated precipitation from rates greater than 50 mm d^{-1} (PI intervals of 5 cm) from (Figures 7a, 7c, and 7e) CAM and (Figures 7b, 7d, and 7f) SPCAM three-hourly output; black line shows Rocky Mountain ridgeline.

maximum, are consistent with the regional changes and the differences between CAM and SPCAM over North America described earlier.

In summary, changes in mean rainfall are associated with regional circulation and moisture anomalies, which manifest differently in CAM and SPCAM, despite the constrained boundary condition forcing across PI versus 4×CO$_2$ simulation end members. CAM is much more dynamically sensitive to 4×CO$_2$ in the vicinity of the jet streak east of the Rockies than SPCAM, with a response promoting onshore southeasterly flow that may help supply moisture for Eastern United States rainfall. A weaker dynamical anomaly in SPCAM is

more regionally confined, and does not extend over the Atlantic Ocean, such that northerly flow along the east coast instead brings cold dry air to the Eastern United States region. Both models predict an intensification of the Central United States southerly low-level jet, but it is stronger in SPCAM than CAM, coincident with a regional moisture increase. Vertical wind shear across North America reduces more in CAM in association with greater high-latitude warming (polar amplification) and larger geopotential height anomalies which may be related to a significant change in the planetary thermal wind balance affecting large-scale circulation such as a broadening and weakening of the zonal mean circulation pattern.

4. Changes in Rainfall and Convective Storm Intensity

4.1. Changes in Rainfall Rates

Previous work summarized in the introduction has suggested that changes in the large-scale environment, such as the vertical wind shear and strength of the low-level jet described above, as well as increases in CAPE and low-level moisture, can impact the intensity and timing of precipitation. And although differences in the mean precipitation response to climate change between CAM and SPCAM revealed complex patterns of change associated with circulation, the projected changes in rainfall intensity are more straightforward to interpret. The analysis in this section shows a consistent effect of superparameterization, regardless of the mean changes.

Figures 7 and 8 compare two metrics of the response of rainfall variability—the contribution to seasonal accumulated rainfall from rain rates above versus below a threshold (Figure 7; 50 mm d^{-1}) and changes in percentile precipitation rates (Figure 8; 50th, 75th, and 99th). Heavy rain rates do not play a major role in mediating seasonal mean rainfall in CAM, but do have a nontrivial effect in SPCAM. The CAM simulations do not produce a significant amount of rain over the United States from rates above 50 mm d^{-1}. Nowhere over the domain does the PI seasonal accumulated contribution reach more than 5 cm, and therefore not much change is shown in Figure 7e. The total accumulated change in CAM results almost entirely from changes in lower precipitation rates, which show the same pattern as the mean change (Figures 7a and 7c). The same result is depicted in changes in the 75th percentile precipitation rates, which have a similar pattern as the mean change (Figure 8c). Changes at lower (50th) percentile precipitation rates capture the onshore shift in Gulf Stream rainfall and reduction in the Central United States maximum. Changes in higher (99th) percentiles show a small reduction across the entire Central-Eastern United States in CAM. While SPCAM produces the opposite response with a substantial increase (decrease) in the contribution of seasonal rain from rates above (below) 50 mm d^{-1} and higher (lower) percentile precipitation rates. The most significant increases in precipitation rates in SPCAM occur over Texas and extend into the Central United States, where moisture and humidity were shown to increase, as discussed above. Decreased rain from lower precipitation rates is seen over most of the Eastern United States, and most significantly over the Southeast United States and the Gulf Stream.

Focusing on the especially interesting region of discrepant model predictions of convective variability in the Central-Eastern United States land (orange box in Figures 7 and 8) and collapsing Figure 8 into a single probability density function (PDF) of precipitation rate (Figure 9a) shows a robust shift toward more intense precipitation in SPCAM with quadrupled CO$_2$. This shift in the tail of the PDFs is brought out clearly with exponential bin spacing (10$^{0.1}$ mm d^{-1}) and is greater than the overlapping range of the interannual 5 year standard deviation, and thus seems statistically robust. In this region, SPCAM has an overall reduction in total seasonal rainfall of 4.1 cm (Table 1), but the rain amount distribution [*Pendergrass and Hartmann*, 2014b] shows an increase in the accumulated amount of rain from rates above 40 mm d^{-1} (Figure 9b). CAM shows very little change in both the total seasonal rainfall and the PDF of rain rates. Although not outside the range of interannual variability, CAM has a small reduction in accumulated rain from the highest rain rates and an increase from weaker rates in the 5 year periods.

This analysis has intentionally focused on North America, where SPCAM's representation of diurnal convection variability in the present climate has previously been validated, but the question naturally arises as to whether amplified extreme rainfall is consistently predicted for other regions. To investigate this issue, Figure 10 briefly expands the rainfall PDF analysis to include several other Northern Hemisphere regions known for organized propagating convection (Southeast Asia and West Africa) [*Stensrud*, 1996] as well as all boreal summer land. The overall result shows an intensification of summertime rainfall extremes is
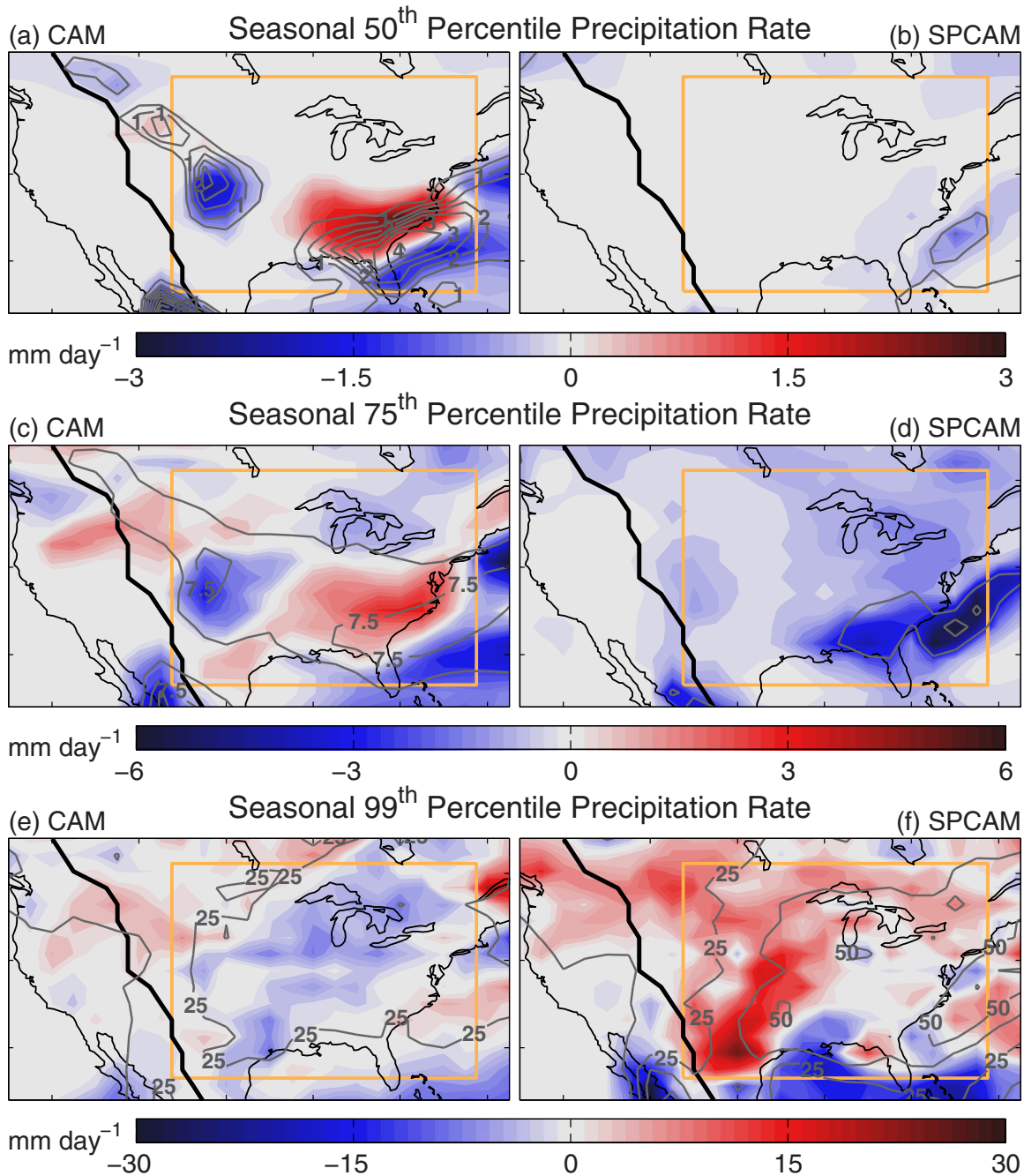
Figure 8. A 5 year seasonal (MJJA) PI (contours) and the difference between $4\times$ and PI (colors) (a and b) 50th (PI intervals of 0.5 mm d^{-1}), (c and d) 75th (PI intervals of 3.75 mm d^{-1}), and (e and f) 99th (PI intervals of 12.5 mm d^{-1}) percentile precipitation rates from (Figures 8a, 8c, and 8e) CAM and (Figures 8b, 8d, and 8f) SPCAM three-hourly output; black line shows Rocky Mountain ridgeline.

simulated by SPCAM over all three landmasses, which tends to agree with basic climate theory about the expected response of extreme rainfall to climate change. It is interesting that in SPCAM the West African rainfall response is especially strong, given that the model explicitly resolves African Easterly Waves [*McCrary*, 2012]. The inability of CAM to capture a significant shift in the rainfall PDF is also a general phenomenon seen in all regions. Broader conclusions based on these other regions will depend on a detailed analysis of present-day hydrologic variability there, which is left for future work. In the meantime, this preliminary analysis suggests the intensification of rainfall simulated by SPCAM over the United States is a robust response to the $4\times CO_2$ forcing.
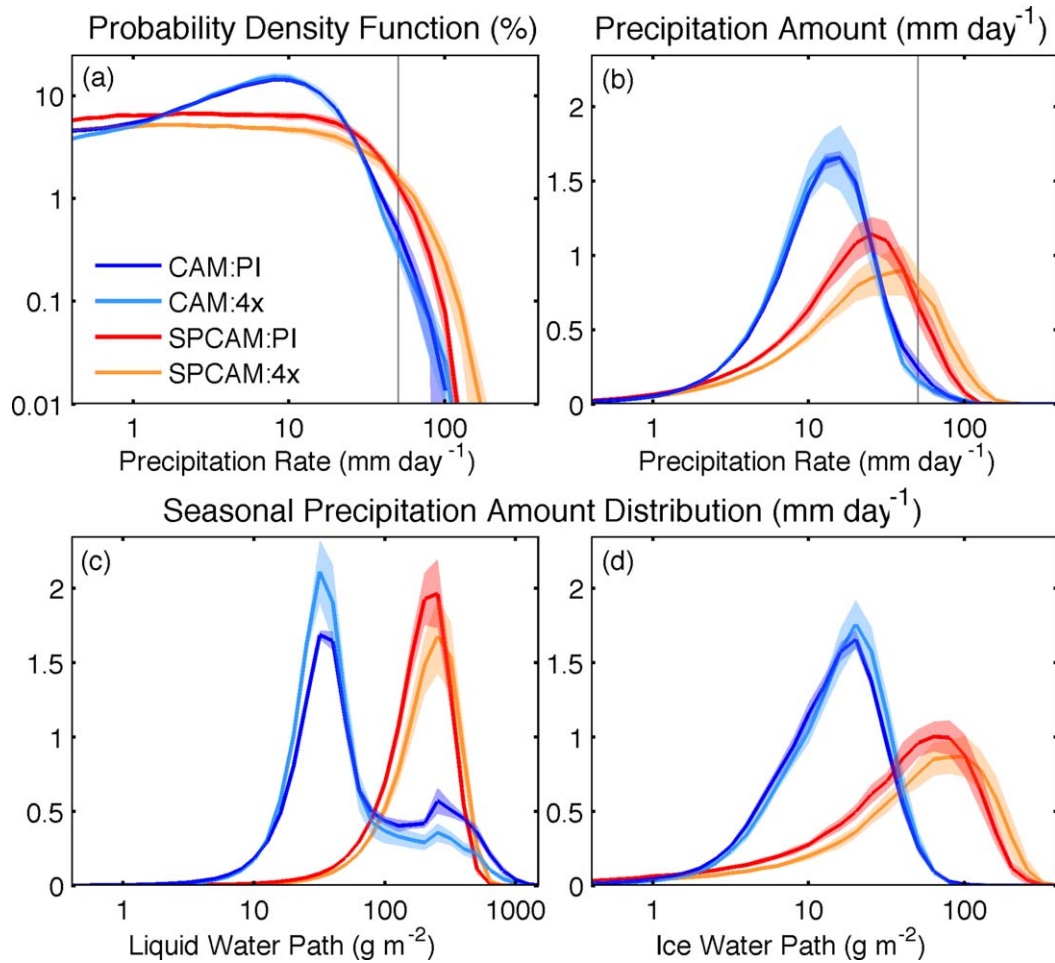
Figure 9. A 5 year seasonal (MJJA) Central-Eastern United States (a) probability density function (%) and (b–d) precipitation amount distribution (mm d^{-1}) as a function of (Figures 9a and 9b) precipitation rate, (Figure 9c) liquid water path, and (Figure 9d) ice water path from CAM and SPCAM PI (blue and red) and 4x (aqua and orange) three-hourly output; with exponential bin spacing in increments of $10^{0.1}$ mm d^{-1} and g m^{-2}; for the region shown in Figures 7 and 8, only including land points; shading indicates annual standard deviation of the 5 year seasonal (MJJA) member ensemble.

The shift toward higher rates with warmer climate in SPCAM is accompanied by an increase in the amount of rain from more extreme liquid and ice water path values (Figures 9c and 9d) over Central-Eastern United States land, which shift toward higher values, but decrease overall by -8.1 and -0.7 g m^{-2}, respectively. CAM has an even larger overall reduction in liquid water path of -13.1 g m^{-2}, but results in a decrease (increase) in the amount of rain from higher (lower) values (Figure 9c). Yet curiously, CAM shows more rain from higher ice water path values similar to SPCAM (Figure 9d). This conflicting response in CAM, more rain from lower liquid water paths and higher ice water paths, is explained by a change in the partitioning between parameterized deep convection and resolved large-scale precipitation. Although the total precipitation only changes by a small amount in CAM, convective precipitation increases by 3.0 cm balancing a -2.9 cm decrease in large-scale precipitation (Table 1). The higher ice water path values are associated with deep convection and higher liquid water path values are associated with large-scale precipitation.

This pattern can be seen in PDFs of the accumulated precipitation as a function of precipitation rate, and liquid and ice water paths, separating convective and large-scale contributions, shown in Figure 11. In the Central-Eastern United States summer, where smaller-local and mesoscale-propagating convective systems are the dominant source of rain in nature, large-scale precipitation in CAM generates the most intense rainfall and is associated with extreme values in liquid water path (this is also true for global-annual PDFs, not shown). This may be expected for other regions or seasons when the majority of rainfall is generated by synoptic frontal systems, providing a large-scale saturated environment and resolved-scale moist overturning, but is counterintuitive for Central-Eastern United States land in summer. It appears the opposite

Table 1. PI and the Difference Between 4× and PI Simulations for Area-Weighted Mean Surface Temperature, Surface Humidity, Precipitable Water, Liquid Water Path, Ice Water Path, Evaporation, and Precipitation (Total, Convective, and Large Scale) for CAM and SPCAM in the Region Shown in Figures 7 and 8, Including Only Points Over Land

	CAM		SPCAM	
	PI	4×–PI	PI	4×–PI
Surface temperature (°C)	20.5	6.6	22.1	6.6
Near-surface humidity (g kg^{-1})	10.2	2.8	9.7	2.1
Precipitable water (kg m^{-2})	25.9	9.5	28.0	9.1
Liquid water path (g m^{-2})	47.1	−13.1	43.2	−8.1
Ice water path (g m^{-2})	5.4	0.1	11.1	−0.7
Evaporation (cm)	41.8	−0.1	38.3	−2.2
Total precipitation (cm)	41.6	0.0	33.8	−4.1
Convective precipitation (cm)	35.6	3.0	N.A.	N.A.
Large-scale precipitation (cm)	5.9	−2.9	N.A.	N.A.

response in CAM is related to the fact that large-scale precipitation controls the tails of its rainfall PDFs (extreme rain), and the artificial separation between large-scale and deep convective precipitation in CAM (at least at this coarse resolution) may decouple rainfall extremes from important climate change drivers (e.g., subgrid-scale moisture convergence and CAPE). Counterintuitively, an increase in extreme rain would occur in CAM only if the conditions that generate large-scale resolved saturated uplift increase; increases in factors affecting the deep convection parameterization do not impact the heaviest rain rates. The reduced equator-to-pole temperature gradient, baroclinicity, vertical wind shear, and overall liquid water path, described above, may instead contribute to a reduction in large-scale (extreme) rainfall.

4.2. Mesoscale Convective Storms

Propagating mesoscale convective systems (MCSs) are a major source of not only total rainfall for the Central United States, but also the most intense rainfall rates [*Schumacher and Johnson*, 2005]. One of the novel features of SPCAM is its ability to capture MCSs [*Kooperman et al.*, 2013; *Pritchard et al.*, 2011]. It is logical to suspect they play a role in mediating convective variability sensitivity to climate change, as the Central United States is also where the two models disagree most drastically in their 99th percentile precipitation rate response to 4×CO$_2$ (Figures 9e and 9f), which shows a reduction from Texas stretching across the Central United States and over the Great Lakes in CAM and an opposite increase across the same region in SPCAM.

The change in mesoscale convective storm activity from PI to 4×CO$_2$ climates is thus evaluated in this section following the MCS index method described in *Kooperman et al.* [2013]. In this approach, an empirical orthogonal function (EOF) based index, similar to that developed by *Wheeler and Hendon* [2004] for the Madden-Julian Oscillation, is used to identify MCS events and composite their propagation by phase. *Kooperman et al.* [2013] show that the MCS signal is not captured in conventional versions of CAM, but exists in several versions of SPCAM, and is most realistic in version 5 used here.

The index is based on 23 years of longwave cloud forcing observations from the NASA Global Energy and Water Cycle Experiment, Surface Radiation Budget (SRB) version 3.1 [*Stackhouse et al.*, 2011], which is band-pass filtered for 12–48 h time scales and meridionally averaged in the Central United States (orange box in Figures 12e–12l). EOF analysis is applied to the filtered signal from observations and the model results are regressed onto the spatial patterns of the first and second leading EOF pair. The MCS index is calculated by transforming the principal component time series into polar coordinates as depicted in the phase diagrams shown in Figures 12a–12d), where the amplitude is the distance from the center ($\sqrt{PC_1^2 + PC_2^2}$) and phase (1–8) is the angular relationship. Events are determined by three criteria: (1) at least three (9 h) consecutive index amplitudes greater than 0.15 propagating forward (east) in phase space, (2) spanning at least 70% of the domain, and (3) starting between 6 P.M. and 3 A.M. local (CST) time. Applying these rules 84, 79, 20, and 19 events are identified in SPCAM:PI, SPCAM:4×, CAM:PI, and CAM:4×, respectively, over the five MJJA seasons, which trace events starting in phases 1 and 2 (green) and ending in phases 7 and 8 (red) in Figures 12a–12d. Composite analysis by phase reveals that the events identified in CAM do not represent active convective and precipitating systems, but are rather advected condensate (not shown, see *Kooperman et al.* [2013]).
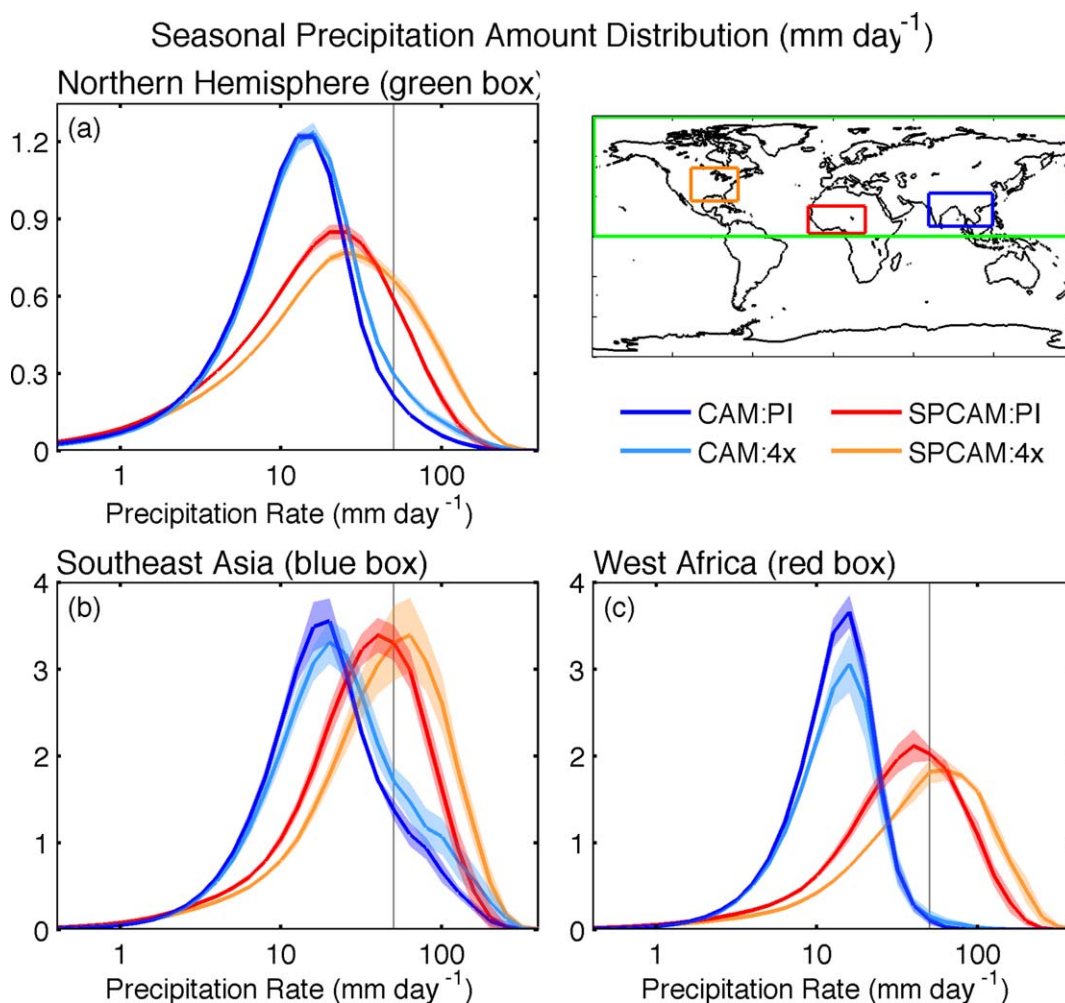
Figure 10. Same as Figure 9b—seasonal precipitation amount distribution, but for three other regions including (a) the Northern Hemisphere, (b) Southeast Asia, and (c) West Africa, only including land points.

The composite results for SPCAM in Figures 12e–12l show an eastward propagating system with increasing phase in both the PI and $4\times CO_2$ simulations. In both simulations the composite system enters the western boundary in phases 1/2 and reaches the eastern side in phases 7/8, with rain beginning in phases 1/2 and intensifying during the middle (nocturnal) phases. Rainfall appears to extend to the Southeast United States in phases 7/8, but is due to a projection of the diurnal timing of rainfall over the Southeast onto the composite timing of phases 7/8, and is not part of the Central United States propagating system. A clear amplification of the composite storm can be seen with the addition of $4\times CO_2$. The system is much broader in all phases and increases the magnitude (15 W m^{-2}) of longwave cloud forcing in phases 5 through 8. Likewise, precipitation increases during all phases, with a maximum in phases 5/6, increasing significantly from ~11 mm d^{-1} in the PI simulation to ~15 mm d^{-1} in the $4\times CO_2$ simulation. This result is consistent with the intensification of the low-level jet and Central United States moisture anomalies discussed above, but a full composite analysis of the processes contributing to amplified MCS activity will be the focus of future work.

Changes in MCS storm intensity are one manifestation of a more general shift toward higher rain rates in SPCAM, at all times of day. Focusing on the Central United States region (left side of the orange box in Figures 12e–12l), rain rate PDFs are recreated in Figure 13 unfolding the diurnal signature of rainfall intensity changes. Reduced rain in CAM occurs almost entirely during its overly dramatic afternoon rainfall peak, with little change at other times of day. SPCAM has a more realistically bimodal diurnal rainfall PDF, and although it also projects the largest reduction in afternoon rainfall at moderate rain rates, it projects an increase in heavy rain at all times of day, including the nocturnal component consistent with the MCS amplification
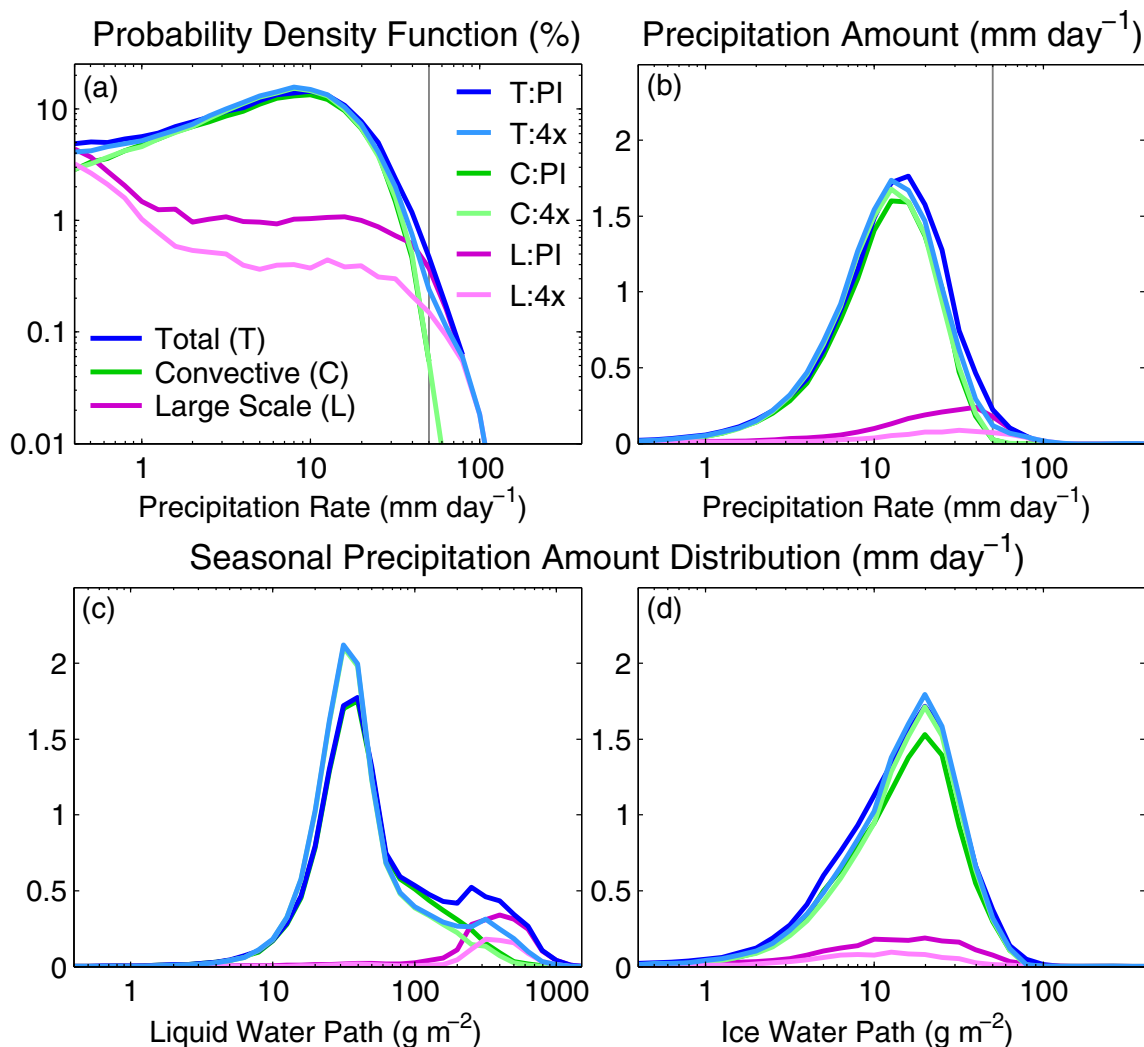
Figure 11. Same as Figure 9, but for CAM only (one MJJA season rerun for additional output) separating the contribution to total precipitation (T-blue) from parameterized convection (C-green) and large-scale (L-purple) precipitation for PI (dark) and 4× (light) simulations.

noted above. The shift in intensity in the afternoon component in this region is consistent with results for the larger Central-Eastern United States region, toward higher rates in SPCAM.

5. Conclusions

In summary, two state of the art climate models—one including a radically updated explicit representation of deep convection—have been analyzed to assess the fast effect of dramatic climate change (4×CO$_2$) on Central United States rainfall and its variability. CAM and SPCAM show similar seasonal mean patterns of change in Alaska and west of the Rockies—regions associated with more large-scale stratiform precipitation, but project a very different hydroclimate response in the Central-Eastern United States—regions where summer rainfall is mostly generated by deeper local and propagating mesoscale convection. The mean precipitation response in this region depends critically on changes in regional circulation patterns that impact the supply of moisture and energy, and respond very differently in the two simulations, suggesting an important role of superparameterization on the dynamic sensitivity of regional circulations. Conventionally parameterized CAM is more dynamically sensitive to climate change in the vicinity of the jet streak downstream of the Rockies, including a widespread increase of southeasterly winds along the United States east coast providing a potential moisture source for increased rainfall there. However, in SPCAM, somewhat more muted dynamical sensitivities are observed along with an increase in mean rainfall in the Central
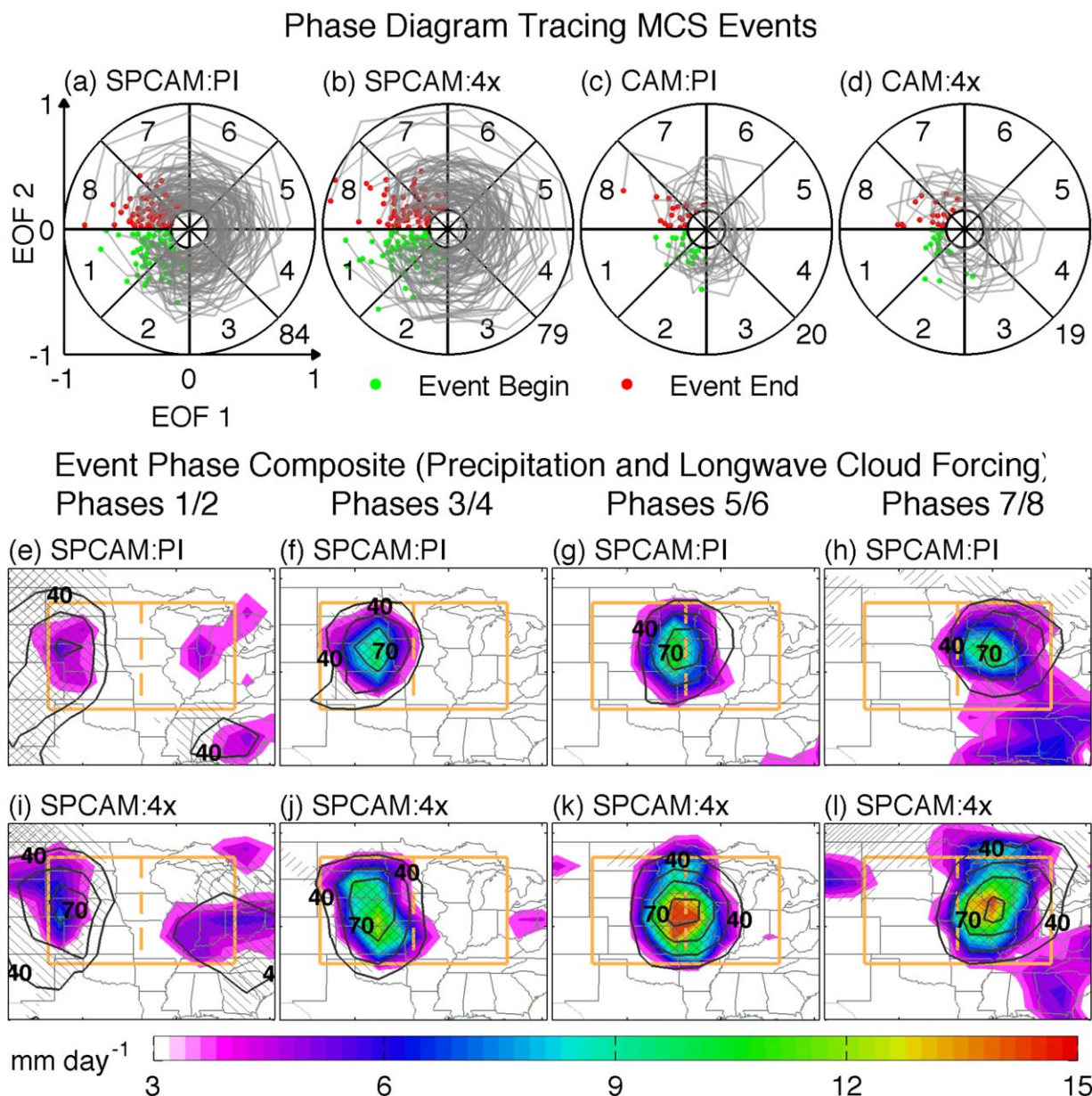
Figure 12. Phase diagram of EOF PC time series 1 and 2 tracing MCS events for (a and b) SPCAM and (c and d) CAM (Figures 12a and 12c) PI and (Figures 12b and 12d) 4× simulations, and composite event phase average of precipitation (colors) and longwave cloud forcing (contours with intervals of 15 W m^{-2}) for phases (e and i) 1 and 2, (f and j) 3 and 4, (g and k) 5 and 6, and (h and l) 7 and 8 in SPCAM (Figures 12e–12h) PI and (Figures 12i–12l) 4× simulations; right/45° (left/−45°) slashes indicate that precipitation (longwave cloud forcing) is significant at 95% confidence interval; depicted as in Figures 2 and 3 from *Kooperman et al.* [2013].

United States linked to an intensification of the low-level jet, and a decrease in rainfall over the east coast coincident with anomalous northerly flow.

The intermodel differences in large-scale circulation anomalies over the United States are linked to a larger planetary response that also exhibits interesting sensitivities to superparameterization. Even when constrained by prescribed sea surface temperatures and sea ice, and springtime initial conditions, the representation of convection can generate nonlocal and global circulation changes that contribute to differences in regional precipitation patterns—an effect that cannot be captured in RCM climate change simulations. In this experiment, CAM has a larger increase in high-latitude temperature (polar amplified warming) with associated geopotential height modulations and a greater expansion and weakening of the Ferrel circulation than SPCAM. This weakens the Northern Hemisphere zonal jet and reduces vertical wind shear across North America more in CAM.
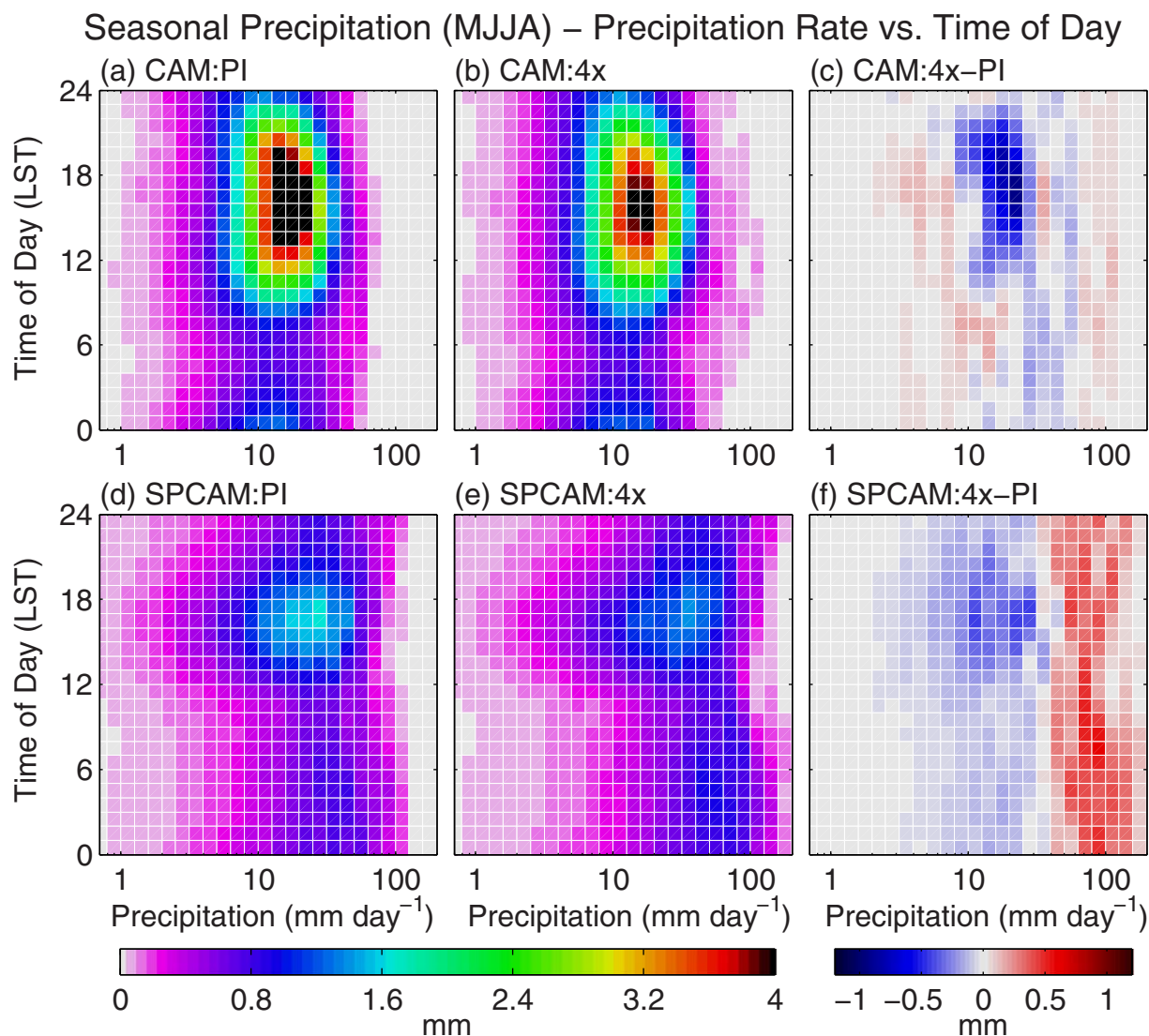
Figure 13. A 5 year seasonal (MJJA) Central-Eastern United States accumulated precipitation (mm) as a joint function of precipitation rate and local time of day for (a and d) PI, (b and e) 4×, and (c and f) the difference between 4× and PI from (Figures 13a–13c) CAM and (Figures 13d–13f) SPCAM simulations; with exponential bin spacing in increments of $10^{0.1}$ mm d^{-1}; for the left-hand side of the region in Figures 12e–12l.

The projected response of rainfall variability and the intensity of extremes to climate change are regionally consistent for each model, despite discrepant predictions of regional mean changes. SPCAM simulations indicate a significant increase in convective storm activity with 4×CO$_2$, projecting greater longwave cloud forcing, precipitation, and storm duration in association with a general increase in overall rainfall intensity throughout the Central-Eastern United States, in line with current theory. On the other hand, CAM does not simulate propagating convective storms and shows an opposite, unexpected effect—a small reduction in rainfall intensity. It is well known that conventionally parameterized GCMs do not simulate extreme precipitation; they rain too weakly and too often compared to observations. Here this is confirmed and it is further illustrated how changes in the extremes in these conventional models may be unrealistically controlled by the physics that affect large-scale (resolved scale) precipitation, rather than environmental parameters affecting subgrid-scale parameterized deep convection. PDF decomposition emphasizes that this factor contributes to the opposite response between the two models and provides some cautionary evidence that even the direction of the change in "what is extreme precipitation for conventional GCMs" may not be reliable in some regions and during some seasons.

One limitation of our experimental design, driving SPCAM with CESM/CAM boundary conditions, is that it leaves open an important question of whether SPCAM would have arrived at a similar climate state had it been allowed to evolve freely in a coupled SPCESM simulation. Such a simulation would be computationally very expensive and is outside the scope of this experiment, but is planned as part of a larger CMMAP initiative. Future work will analyze differences between such a fully coupled SPCESM simulation and the SPCAM results presented here, which will help elucidate the role of differences in long-term planetary feedbacks on United States summer climate from the fast, boundary-driven component analyzed here. Future work will also provide a detailed analysis of MCS composite statistics to identify climate change drivers contributing to storm intensification in SPCAM, and their links to the generation of rainfall extremes in both conventional and superparameterized climate models.

References

Allan, R. P., and B. J. Soden (2008), Atmospheric warming and the amplification of precipitation extremes, *Science*, *321*, 1481–1484.

Allen, M. R., and W. J. Ingram (2002), Constraints on future changes in climate and the hydrologic cycle, *Nature*, *419*, 224–232.

Andrews, T., J. M. Gregory, M. J. Webb, and K. E. Taylor (2012), Forcing, feedbacks and climate sensitivity in CMIP5 coupled atmosphere-ocean climate models, *Geophys. Res. Lett.*, *39*, L09712, doi:10.1029/2012GL051607.

Benedict, J. J., and D. A. Randall (2009), Structure of the Madden-Julian oscillation in the superparameterized CAM, *J. Atmos. Sci.*, *66*(11), 3277–3296.

Brooks, H. E. (2013), Severe thunderstorms and climate change, *Atmos. Res.*, *123*, 129–138.

Bukovsky, M. S., and D. J. Karoly (2011), A regional modeling study of climate change impacts on warm-season precipitation in the Central United States, *J. Clim.*, *24*, 1985–2002.

Carbone, R. E., and J. D. Tuttle (2008), Rainfall occurrence in the US warm season: The diurnal cycle, *J. Clim.*, *21*(16), 4132–4146.

Carbone, R. E., J. D. Tuttle, D. A. Ahijevych, and S. B. Trier (2002), Inferences of predictability associated with warm season precipitation episodes, *J. Atmos. Sci.*, *59*(13), 2033–2056.

Dai, A. (2006), Precipitation characteristics in eighteen coupled climate models, *J. Clim.*, *19*, 4605–4630.

DeMott, C. A., D. A. Randall, and M. Khairoutdinov (2007), Convective precipitation variability as a tool for general circulation model analysis, *J. Clim.*, *20*, 91–112.

Deser, C., A. Phillips, M. Alexander, and B. Smoliak (2013), Projecting North American climate over the next 50 years: Uncertainty due to internal variability, *J. Clim.*, *27*, 2271–2296, doi:10.1175/JCLI-D-13-00451.1.

Grabowski, W. W. (2001), Coupling cloud processes with the large-scale dynamics using the cloud-resolving convection parameterization (CRCP), *J. Atmos. Sci.*, *58*(9), 978–997.

Gregory, J. M., W. J. Ingram, M. A. Palmer, G. S. Jones, P. A. Stott, R. B. Thorpe, J. A. Lowe, T. C. Johns, and K. D. Williams (2004), A new method for diagnosing radiative forcing and climate sensitivity, *Geophys. Res. Lett.*, *31*, L03205, doi:10.1029/2003GL018747.

Held, I. M., and B. J. Soden (2006), Robust responses of the hydrological cycle to global warming, *J. Clim.*, *19*, 5686–5699.

Khairoutdinov, M. F., and D. A. Randall (2001), A cloud resolving model as a cloud parameterization in the NCAR Community Climate System Model: Preliminary results, *Geophys. Res. Lett.*, *28*(18), 3617–3620.

Khairoutdinov, M. F., and D. A. Randall (2003), Cloud resolving modeling of the ARM summer 1997 IOP: Model formulation, results, uncertainties, and sensitivities, *J. Atmos. Sci.*, *60*, 607–625.

Khairoutdinov, M., C. DeMott, and D. Randall (2008), Evaluation of the simulated interannual and subseasonal variability in an AMIP-Style simulation using the CSU multiscale modeling framework, *J. Clim.*, *21*(3), 413–431.

Khairoutdinov, M., D. Randall, and C. DeMott (2005), Simulations of the atmospheric general circulation using a cloud-resolving model as a super-parameterization of physical processes, *J. Atmos. Sci.*, *62*(7), 2136–2154.

Kooperman, G. J., M. S. Pritchard, and R. C. J. Somerville (2013), Robustness and sensitivities of central U.S. summer convection in the super-parameterized CAM: Multi-model intercomparison with a new regional EOF index, *Geophys. Res. Lett.*, *40*, 3287–3291, doi:10.1002/grl.50597.

Kopparla, P., E. M. Fischer, C. Hannay, and R. Knutti (2013), Improved simulation of extreme precipitation in a high-resolution atmosphere model, *Geophys. Res. Lett.*, *40*, 5803–5808, doi:10.1002/2013GL057866.

Lee, M.-I., S. D. Schubert, M. J. Suarez, I. M. Held, N.-C. Lau, J. J. Ploshay, A. Kumar, H.-K. Kim, and J.-K. E. Schemm (2007), An analysis of the warm-season diurnal cycle over the continental United States and northern Mexico in general circulation models, *J. Hydrometeorol.*, *8*(3), 344–366.

Li, F., D. Rosa, W. D. Collins, and M. F. Wehner (2012), "Super-parameterization": A better way to simulate regional extreme precipitation?, *J. Adv. Model. Earth Syst.*, *4*, M04002, doi:10.1029/2011MS000106.

Li, G., and S. Xie (2013), Tropical biases in CMIP5 multi-model ensemble: The excessive equatorial Pacific cold tongue and double ITCZ problems, *J. Clim.*, *27*, 1765–1780, doi:10.1175/JCLI-D-13-00337.1.

Lin, J.-L., et al. (2006), Tropical intraseasonal variability in 14 IPCC AR4 climate models. Part I: Convective signals, *J. Clim.*, *19*, 2665–2690.

Liu, X., et al. (2012), Toward a minimal representation of aerosols in climate models: Description and evaluation in the community atmosphere model CAM5, *Geosci. Model Dev.*, *5*(3), 709–739.

Maloney, E., et al. (2013), North American climate in CMIP5 experiments: Part III: Assessment of 21st century projections, *J. Clim.*, doi:10.1175/JCLI-D-13-00273.1, in press.

Mapes, B. E., and R. B. Neale (2011), Parameterizing convective organization to escape the entrainment dilemma, *J. Adv. Model. Earth Syst.*, *3*, M06004, doi:10.1029/2011MS000042.

McCrary, R. R. (2012), Seasonal, synoptic and intraseasonal variability of the West African monsoon, PhD dissertation, 160 pp., Colo. State Univ., Fort Collins, Colo.

Mearns, L. O., et al. (2013), Climate change projections of the North American regional climate change assessment program (NARCCAP), *Clim. Change*, *120*, 965–975.

Moncrieff, M. W. (1992), Organized convective systems: Archetypal dynamic-models, mass and momentum flux theory, and parametrization, *Q. J. R. Meteorol. Soc.*, *118*(507), 819–850.

Moncrieff, M. W. (2010), The multiscale organization of moist convection at the intersection of weather and climate, in Why Does Climate Vary?, Editors D.-Z. Sun, and F. Bryan, *Geophys. Monogr. Ser.*, vol. 189, pp. 3–26, AGU, Washington, D. C.

Morrison, H., and A. Gettelman (2008), A new two-moment bulk stratiform cloud microphysics scheme in the community atmosphere model, version 3 (CAM3). Part I: Description and tests, *J. Clim.*, *21*, 3642–3659.

Muller, C. J., P. A. O'Gorman, and L. E. Back (2011), Intensification of precipitation extremes with warming in a cloud-resolving model, *J. Clim.*, *24*, 2784–2800.

Neale, R. B., et al. (2010), *NCAR Technical Note: Description of the NCAR Community Atmosphere Model (CAM 5.0)*, Natl. Cent. for Atmos. Res., Boulder, Colo.

O'Gorman, P. A. (2012), Sensitivity of tropical precipitation extremes to climate change, *Nat. Geosci.*, *5*, 697–700.

O'Gorman, P. A., and T. Schneider (2009a), The physical basis for increases in precipitation extremes in simulations of 21st-century climate change, *Proc. Natl. Acad. Sci. U. S. A.*, *106*(35), 14,773–14,777.

O'Gorman, P. A., and T. Schneider (2009b), Scaling of precipitation extremes over a wide range of climates simulated with an idealized GCM, *J. Clim.*, *22*, 5676–5685.

Park, S., and C. S. Bretherton (2009), The University of Washington shallow convection and moist turbulence schemes and their impact on climate simulations with the community atmosphere model, *J. Clim.*, *22*(12), 3449–3469.

Patricola, C. M., and K. H. Cook (2013a), Mid-twenty-first century warm season climate change in the Central United States. Part I: Regional and global model predictions, *Clim. Dyn.*, *40*, 551–568.

Patricola, C. M., and K. H. Cook (2013b), Mid-twenty-first century climate change in the Central United States. Part II: Climate change processes, *Clim. Dyn.*, *40*, 569–583.

Pendergrass, A., and D. Hartmann (2014a), The atmospheric energy constraint on global-mean precipitation change, *J. Clim.*, *27*, 757–768, doi:10.1175/JCLI-D-13-00163.1.

Pendergrass, A., and D. Hartmann (2014b), Two modes of change of the distribution of rain. *J. Clim.*, submitted. (http://www.atmos.washington.edu/~dennis/pendergrasshartmannsubmittedp1.pdf)

Pritchard, M. S., and R. C. J. Somerville (2009), Assessing the diurnal cycle of precipitation in a multi-scale climate model, *J. Adv. Model. Earth Syst.*, *1*, 12, doi:10.3894/JAMES.2009.1.12.

Pritchard, M. S., M. W. Moncrieff, and R. C. J. Somerville (2011), Orogenic propagating precipitation systems over the United States in a global climate model with embedded explicit convection, *J. Atmos. Sci.*, *68*(8), 1821–1840.

Randall, D., M. Khairoutdinov, A. Arakawa, and W. Grabowski (2003), Breaking the cloud parameterization deadlock, *Bull. Am. Meteorol. Soc.*, *84*(11), 1547–1564.

Romps, D. M. (2011), Response of tropical precipitation to global warming, *J. Atmos. Sci.*, *68*, 123–138.

Rosa, D., and W. D. Collins (2013), A case study of sub-daily simulated and observed continental convective precipitation: CMIP5 and multiscale global climate models comparison, *Geophys. Res. Lett.*, *40*, 5999–6003, doi:10.1002/2013GL057987.

Scheff, J., and D. Frierson (2012), Robust future precipitation declines in CMIP5 largely reflect the poleward expansion of model subtropical dry zones, *Geophys. Res. Lett.*, *39*, L18704, doi:10.1029/2012GL052910.

Schumacher, R. S., and R. H. Johnson (2005), Organization and environmental properties of extreme-rain-producing mesoscale convective systems, *Mon. Weather Rev.*, *133*, 961–976.

Smith, A., and R. Katz (2013), U.S. billion-dollar weather and climate disasters: Data sources, trends, accuracy and biases, *Nat. Hazards*, *67*, 387–410.

Solomon, S., D. Qin, M. Manning, Z. Chen, M. Marquis, K. B. Averyt, M. Tignor, and H. L. Miller (Eds.) (2007), *Climate Change 2007: The Physical Science Basis. Contribution of Working Group I to the Fourth Assessment Report of the Intergovernmental Panel on Climate Change*, Cambridge Univ. Press, Cambridge, U. K.

Stackhouse, P. W., Jr., S. K. Gupta, S. J. Cox, T. Zhang, J. C. Mikovitz, and L. M. Hinkelman (2011), 24.5-year SRB data set released, *GEWEX News*, *21*(1), 10–12.

Stensrud, D. J. (1996), Importance of low-level jets to climate: A review, *J. Clim.*, *9*, 1698–1711.

Stephens, G. L., and T. D. Ellis (2008), Controls of global-mean precipitation increases in global warming GCM experiments, *J. Clim.*, *21*, 6141–6155.

Stephens, G. L., T. L'Ecuyer, R. Forbes, A. Gettelmen, J.-C. Golaz, A. Bodas-Salcedo, K. Suzuki, P. Gabriel, and J. Haynes (2010), Dreary state of precipitation in global models, *J. Geophys. Res.*, *115*, D24211, doi:10.1029/2010JD014532.

Stocker, T. F., D. Qin, G.-K. Plattner, M. Tignor, S. K. Allen, J. Boschung, A. Nauels, Y. Xia, V. Bex, and P. M. Midgley (Eds.) (2013), *Climate Change 2013: The Physical Science Basis. Contribution of Working Group I to the Fifth Assessment Report of the Intergovernmental Panel on Climate Change*, Cambridge Univ. Press, Cambridge, U. K.

Stouffer, R. J., et al. (2006), Investigating the causes of the response of the thermohaline circulation to past and future climate changes, *J. Clim.*, *19*, 1365–1387.

Sun, Y., S. Solomon, A. Dai, and R. W. Portmann (2006), How often does it rain?, *J. Clim.*, *19*, 916–934.

Thayer-Calder, K., and D. A. Randall (2009), The role of convective moistening in the formation and progression of the MJO, *J. Clim.*, *66*, 3297–3312.

Trapp, R. J., N. S. Diffenbaugh, and A. Gluhovsky (2009), Transient response of severe thunderstorm forcing to elevated greenhouse gas concentrations, *Geophys. Res. Lett.*, *36*, L01703, doi:10.1029/2008GL036203.

Trenberth, K. E. (2011), Changes in precipitation with climate change, *Clim. Res.*, *47*, 123–138.

Trenberth, K. E., A. Dai, R. M. Rasmussen, and D. B. Parsons (2003), The changing character of precipitation, *Bull. Am. Meteorol. Soc.*, *84*, 1205–1217.

Wang, M., et al. (2011), The multi-scale aerosol-climate model PNNL-MMF: Model description and evaluation, *Geosci. Model Dev.*, *4*(1), 137–168.

Wehner, M. F. (2013), Very extreme seasonal precipitation in the NARCCAP ensemble: Model performance and projections, *Clim. Dyn.*, *40*, 59–80.

Wehner, M. F., R. L. Smith, G. Bala, and P. Duffy (2010), The effect of horizontal resolution on simulation of very extreme US precipitation events in a global atmosphere model, *Clim. Dyn.*, *34*, 241–247.

Wheeler, M. C., and H. H. Hendon (2004), An all-season real-time multivariate MJO index: Development of an index for monitoring and prediction, *Mon. Weather Rev.*, *132*, 1917–1932.

Wilcox, E. M., and L. J. Donner (2007), The frequency of extreme rain events in satellite rain-rate estimates and an atmospheric general circulation model, *J. Clim.*, *20*(1), 53–69.

Zhang, G. J., and N. A. McFarlane (1995), Sensitivity of climate simulations to the parameterization of cumulus convection in the Canadian climate center general-circulation model, *Atmos. Ocean*, *33*(3), 407–446.